ACS APPLIED NANO MATERIALS

www.acsanm.org
Article

Extracellular Vesicle-Liposome-Darunavir Formulation for the Treatment of HIV Neuropathogenesis

Lina Zhou, Sandip Godse, Namita Sinha, Dejian Ma, Golnoush Mirzahosseini, Mohd Salman, Paul Pulliam, Chalet Tan, Udai P. Singh, Tauheed Ishrat, Harry Kochat, and Santosh Kumar*

Cite This: *ACS Appl. Nano Mater.* 2025, 8, 6857−6876

ABSTRACT: This study evaluates the efficacy of an extracellular vesicles-liposome-darunavir (EV-Lip-DRV) formulation for the treatment of HIV neuropathogenesis, including neurocognitive disorders. The EV-Lip-DRV formulation was developed through a process involving thin-film hydration and extrusion, followed by ultrafiltration to remove unloaded DRV. The encapsulation efficiency was found to be 41.75 ± 2.19%, with a particle size of ∼189 nm and zeta potential of ∼−7.8 mV. The hemocompatibility test confirmed the safety of the formulation for red blood cells, while drug release profiles demonstrated a sustained release of DRV within 24 h. Our *in vitro* experiment showed that EV-Lip-DRV significantly reduces HIV replication in U1 macrophages and alters the pro-inflammatory cytokine and chemokine levels. Pharmacokinetic studies in C57BL/6 mice via intranasal administration revealed significantly enhanced drug delivery in the brain, relative to systemic circulation and other peripheral organs. Behavioral studies using EcoHIV-infected mice indicated significant improvements in HIV-associated impaired cognitive and motor functions when treated with the EV-Lip-DRV formulation compared to those with DRV alone. Furthermore, analysis of brain tissues from these mice showed significantly reduced HIV-associated inflammatory response, oxidative stress, DNA damage, and neuronal damage in EV-Lip-DRV as compared with DRV alone. Taken together, these findings suggest that EV-Lip is a promising vehicle for enhancing the delivery of antiretroviral drugs to the brain, potentially ameliorating symptoms associated with HIV neuropathogenesis and improving overall outcomes in HIV treatment.

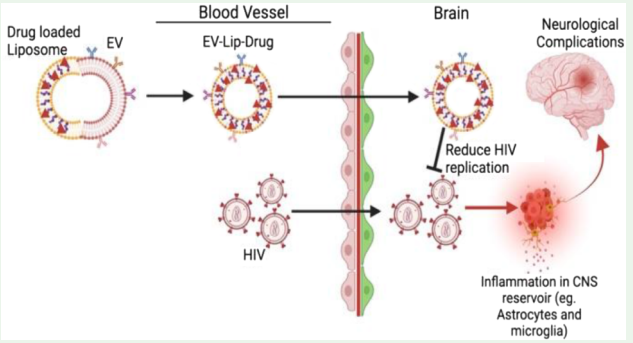

KEYWORDS: *extracellular vesicles, liposomes, antiretroviral therapy, intranasal drug delivery, HIV neuropathogenesis*

1. INTRODUCTION

The availability and accessibility of antiretroviral therapy (ART) have greatly increased since the 1990s, resulting in improved health outcomes and increased life expectancy for people living with the human immunodeficiency virus (HIV). Despite significant advances in treatment, a complete cure for HIV is yet to be developed. HIV continues to be a major global health concern, affecting approximately 38.4 million individuals worldwide as of 2021. With the progression of HIV, 42.6% of patients are suffering from HIV-associated neurocognitive disorder (HAND) and dysfunctions such as dementia, impaired memory, cognitive impairment, etc.[1]

HIV can be detected in the cerebrospinal fluid (CSF) remarkably early in the course of infection, potentially as soon as 8 days after transmission.[2] This early penetration of HIV into the central nervous system (CNS) underscores the virus's capacity to establish the infection beyond the primary immune defense systems. HIV replication within the CNS primarily occurs in perivascular macrophages and microglia, triggering a significant innate immune response.[3] This response is characterized by the production of inflammatory factors such as cytokines and chemokines, along with oxidative stress, all of which contribute to the development of HAND.[3] Astrocytes also play a crucial role by supporting low-level HIV replication, which allows the virus to persist and potentially establish a latent infection within the CNS.[4] Effective suppression of HIV in the HIV reservoirs in the brain hinges on maintaining optimal concentrations of ART drugs. However, the blood−brain barrier (BBB) poses a significant challenge in this context.[5] Furthermore, the susceptibility of the ART drugs to efflux transporters, including multidrug resistance protein 1 (MRP1) and P-glycoprotein (P-gp), further impedes their ability to penetrate the BBB.[5] Consequently, achieving

Received: August 13, 2024
Revised: February 21, 2025
Accepted: February 27, 2025
Published: April 1, 2025

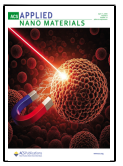

https://doi.org/10.1021/acsanm.4c04637
ACS Appl. Nano Mater. 2025, 8, 6857−6876

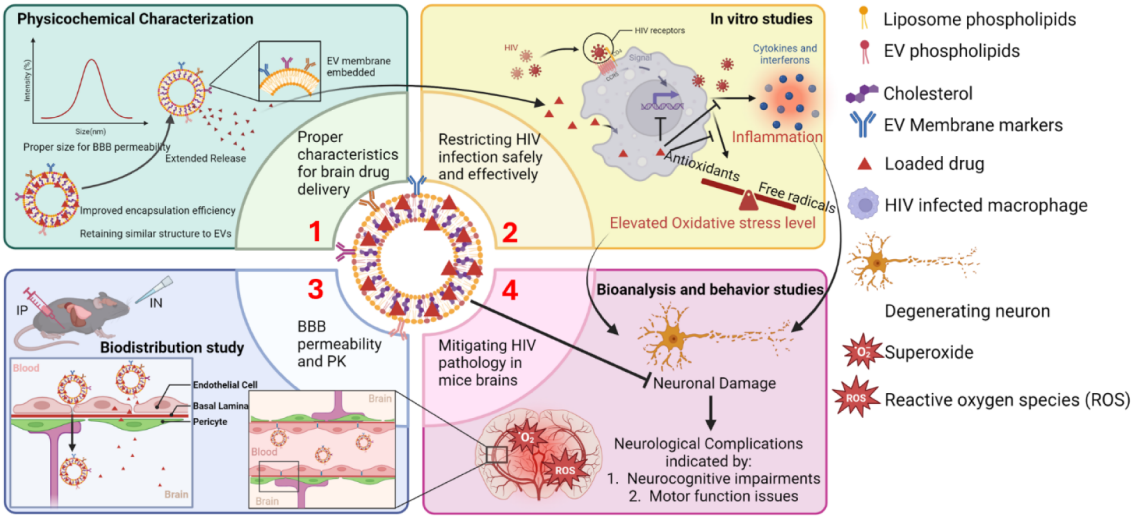

Figure 1. Schematic abstract of the study. We developed an EV-Lip-DRV formulation and characterized its physicochemical profiles. We also studied the in vitro release profile and efficacy of EV-Lip-DRV on restricting the HIV replication in HIV-infected cells. Further, we studied drug delivery profile in wild-type and neuropathological and behavioral effects of EV-Lip-DRV in EcoHIV mice.

therapeutic levels of ART drugs in the brain is challenging, complicating efforts to suppress HIV replication in this critical reservoir and highlighting the need for a safer and more effective drug delivery system (DDS) to enhance drug delivery across the BBB.

Extracellular vesicles (EVs) are small, lipid bilayer-encapsulated particles released by cells into the extracellular environment and found in various biological fluids such as blood, urine, and cerebrospinal fluid.[6] These membrane-bound particles facilitate targeted delivery of molecular cargo to their originating cells, enabling precise intercellular communication.[6] EVs are categorized mainly into exosomes (30−150 nm), microvesicles (100−1000 nm), and apoptotic bodies (1−5 nm), based on their size and origin. For brain drug delivery, EVs within 200 nm of size are considered appropriate.[7] However, a low percentage of encapsulation efficiency (EE%) of the EV formulation poses a challenge for in vitro and in vivo studies.[7,8] A liposome is a small artificial nanoparticle composed of at least one synthetic phospholipid bilayer. It has been approved by the FDA as a safe carrier for small molecules with a sufficient EE%. In the case of doxorubicin, the EE% can be more than 90%.[9]

Recently, to overcome the low encapsulation efficiency in EVs, an EV-Lip hybrid system was developed and introduced to the field of targeted drug delivery. Small molecules and genes have been loaded into EV-liposome hybrid nanoparticles to treat bone loss,[10] cancer,[11] pulmonary fibrosis, etc. Other than the EV-Lip hybrid system, studies have shown that the liposome-cell membrane hybrid system can deliver cancer therapy to the target site at a relatively high EE%.[12] Goh et al. have established a drug delivery platform named nano cell vesicle technology systems (nCVTs), which combines cell membranes from U937 monocytes with synthetic lipids to create a targeted delivery mechanism for tumor sites. By retaining essential surface proteins from U937 monocytes and incorporating liposomal elements, nCVTs enhance targeting and cellular uptake, while minimizing immunogenicity. However, the EE% of the nCVT is up to 20%, highlighting the need for substantial optimization to improve its EE% to proceed in the clinical setting. Researchers also strived to make synthetic or bottom-up assembled EV-like liposomes to optimize the biocompatibility of the nanoparticle.[13] This is a promising field; however, it also requires techniques to identify the membrane components of EVs for mimicking to optimize the components of the membrane lipids and membrane proteins for targeted drug delivery.

The scope of our study is depicted in Figure 1. The long-term goal is to develop a scalable, feasible, and cost-efficient EV-based nanoparticle drug delivery system to treat HIV neuropathogenesis including HAND. First-line of HIV therapies often includes the nucleoside reverse transcriptase inhibitors (NRTIs) lamivudine and emtricitabine/tenofovir (FTC/TDF)[14] with or without DRV. While ritonavir (RTV) is generally used as pharmaco-enhancers of DRV,[15] the need for RTV is likely to be eliminated in DRV nanoformulation, which is expected to largely bypass drug metabolism. Although all ART drugs induce oxidative stress and neuronal damage,[16] even high doses of DRV are relatively safe.[17] Moreover, the slight ability of DRV to cross the BBB[18] makes it an attractive candidate for use in the brain. Previous study has also led to the development of nanoformulations with DRV for use in treating HIV in brain reservoirs.[19] Therefore, this study focuses on the development of an EV-Lip hybrid nanoparticle with encapsulated DRV to improve its distribution in the brain and ameliorate HIV neuropathogenesis, including cognitive disorders. We developed an EV-Lip-DRV formulation and assessed its antiretroviral efficacy in vitro using U1 cells, which are a human monocytic cell line derived from U937 cells that have been chronically infected with HIV-1, and the capability of the EV-Lip-DRV formulation to deliver DRV to the brain and alleviate HAND-related symptoms in animal models of HIV neuropathogenesis.

2. MATERIALS AND METHODS

2.1. Materials. 1,2-Dioleoyl-*sn*-glycero-3-phosphocholine (DOPC, 850375), cholesterol (700100), 16:0−06:0 NBD PC (810130), and 18:1 Liss Rhod PE (810150) were purchased from Avanti Polar Lipids (Birmingham, AL, USA). DRV (TRC-D193500) was purchased from Toronto Research Chemicals, Inc. (North York, ON, Canada). The jacketed extruder (GJE-100 mL) was purchased from Genizer LLC (Los Angeles, CA, USA). Sterile phosphate-buffered saline (PBS) (10100-031) was obtained from Gibco (Dublin,

https://doi.org/10.1021/acsanm.4c04637
ACS Appl. Nano Mater. 2025, 8, 6857−6876

Ireland). L-Glutamine, penicillin−streptomycin solution, LC/MS-grade acetonitrile (A955), formic acid (AC270480010), BD PrecisionGlide 25G needle (14-826-49), and BD 1 mL TB syringe (14-826-88) were obtained from Fisher Scientific (Pittsburgh, PA, USA). Roswell Park Memorial Institute (RPMI) 1640 medium was bought from Corning Inc. (Tewksbury, MA, USA). Fetal bovine serum (FBS) was obtained from Atlanta Biologicals (Atlanta, GA, USA). Dulbecco's modified Eagle's medium (DMEM) was obtained from the American Type Culture Collection. UranyLess (22409) was obtained from Electron Microscopy Science (Hatfield, PA, USA). Constitutively HIV-infected (U1) cell lines were obtained from the NIH AIDS Reagent Program (Germantown, MD, USA). Paraformaldehyde (J19943.K2) and the total exosome isolation kit (from plasma, catalog number 4484450) were purchased from Thermo Fisher Scientific (Waltham, MA, USA).

2.2. Preparation of EV-Liposomes. We sourced EVs from healthy mice plasma and healthy human plasma, selecting based on the intended application: mice plasma-derived EVs for mice studies and human plasma-derived EVs for physicochemical characterization, U1 treatment, and hemolysis studies. EVs were isolated using the total exosome isolation reagent (from plasma) according to the manual provided by the manufacturer. Briefly, the reagent is added to the plasma, and the mixture is incubated for 30 min at 2−8 °C. The precipitated exosomes are then collected by centrifugation at 10,000 × *g* for 5 min at room temperature. The resulting pellet is resuspended in 1 mL 1× PBS. 30 mg of DOPC and cholesterol (70:30 mol %) and 6 mg of DRV were mixed and dissolved in 4 mL of chloroform followed by a thin film of the lipids formed by rotary evaporation at 90 rpm, 40 °C for 3 h. EVs (0.6 mg based on protein amount) in PBS were added into the flask containing the thin film. The mixture was swelled at 40 °C 1 h at 90 rpm. The mixture was subsequently sonicated in a water bath sonicator (Branson Ultrasonics 2800, Brookfield, CT, USA) for 30 s on and 30 s off for 10−15 cycles on ice. Then, the mixture was placed in the water bath at 37 °C for 30 min to allow the liposome to stabilize, reach equilibrium, and interact with the drug compound to enhance the encapsulation efficiency. Following this, the EV and liposome mixture was processed through an extruder for membrane fusion using a series of polycarbonate membrane filters with pore sizes of 0.4 and 0.2 μm at room temperature in nitrogen as the air source. The mixture was processed through each membrane three times, and the suspension was incubated in the water bath at 37 °C for 20 min to facilitate homogenization. Then, the unloaded drug was removed from the EV-Lip formulation by ultrafiltration using an Amicon Ultra Centrifugal Filter (100 kDa MWCO, Millipore Sigma, Burlington, MA, USA) according to the manufacturer's protocol.

2.3. Determination of Morphology by Size, Zeta Potential, and TEM. The average particle size and zeta potential of EV and EV-Lip nanoparticles were measured using dynamic light scattering (DLS) with a Zetasizer (Nano ZS, Malvern Instruments Inc., Malvern, UK). For accurate readings, 50 μL of the formulation was diluted in 850 μL of 1 × PBS (0.22 μm filtered) and placed in a disposable cuvette at room temperature. Zeta potential was calculated using the Smoluchowski equation.

The transmission electron microscope (TEM) analysis was run at 60 kV with a high-resolution digital camera for the morphology of the nanoparticles (JEOL-2000EX, Tokyo, Japan) by the imaging center at UTHSC (Memphis, TN). The EV and EV-Lip samples were diluted (1:500) in dH_2O (0.22 μm filtered). A 10 μL aliquot of the sample was applied to a grid, air-dried, and fixed with Uranyless.

2.4. Proof of Fusion Assay Using Fluorescence Resonance Energy Transfer (FRET). Membrane fusion between EVs and liposomes was assessed by using the FRET technique. Liposomes were incorporated using DOPC, cholesterol, 16:0−06:0 NBD PC, and 18:1 Liss Rhod PE in a molar ratio of 70:30:1:1, and subsequently extruded as previously described. Upon excitation at 460 nm, the emitted energy from NBD-PC at 535 nm was transferred to adjacent Rho-PE through FRET and detected at 580 nm. Fluorescence intensities at both 535 and 580 nm were measured simultaneously using a plate reader (Cytation 5, BioTek, Winooski, VT, USA). In this study, the two fluorophores were positioned on the liposome membranes. As the membranes of the EVs and liposomes fused, the NBD donor and Liss Rhod PE acceptor fluorophores moved apart. This spatial change resulted in increased NBD fluorescence and decreased Liss Rhod PE fluorescence, thereby confirming membrane fusion. The absorbance of H_2O at 585 and 535 nm was used as background. The NBD fluorescence percentage relative to the total absorbance for each sample at 585 and 535 nm was then calculated.

2.5. Quantification of DRV Concentrations. The EV-Lip-DRV formulation was extracted with 10 volumes of acetonitrile to determine the encapsulation efficiency and the measurement of DRV amount in the cell, plasma, and tissue samples using the LC-MS/MS method published earlier.[19,20] The percentage of encapsulation efficiency (EE%) was calculated by the following equation:

$$\text{Encapsulation efficiency}(\%) = \frac{\text{Weight of the drug in nanoparticles}}{\text{Weight of the feeding drugs}} \times 100\%$$

2.6. Measurement of In Vitro Drug Release. The in vitro release profile of EV-Lip-DRV was studied using a method modified from previous publications.[19] Briefly, a total of 5 mL of the EV-Lip-DRV formulation was added to a Float-A-Lyzer dialysis device (8−10 kDa, catalog number Z726508, Sigma-Aldrich, St. Louis, MO, USA). The dialysis device was immersed in 125 mL of 1× PBS at 37 °C. Samples of 20 μL from the reservoir were collected at 5, 15, and 30 min, and 1, 2, 3, 6, 9, 12, 24, 36, 48, 72, and 96 h EV-liposomes. The 1× PBS was replaced every 24 h to maintain the sink condition. The samples collected were spiked in acetonitrile to measure the concentration of DRV by the LC-MS/MS method as previously described.[19]

2.7. Cell Cultures. U1 cells were maintained in RPMI1640 medium prepared with 10% fetal bovine serum (FBS) and 1% L-glutamine. To induce differentiation into macrophages, 0.8 million U1 cells were suspended in 1.5 mL of medium containing 100 nM phorbol 12-myristate 13-acetate (PMA) and plated in 6-well plates. Following a 3-day differentiation period, the medium was removed, and the cells were rinsed with PBS. Then, fresh medium was then added to U1 macrophages, which were incubated for an additional 3−4 h before the treatment.

2.8. LDH Cytotoxicity Assay. Following a daily dose of 6 μg/mL of DRV or EV-Lip-DRV in U1 macrophages, we assessed cytotoxicity levels after 24, 48, and 72 h of treatment using the Pierce Lactate Dehydrogenase (LDH) Cytotoxicity Assay Kit (ThermoFisher Scientific, Grand Island, NY, USA), following the manufacturer's instructions. Briefly, the level of LDH in the cell culture medium indicates cell damage and lysis. We combined 50 μL of the media sample with 50 μL of the LDH assay reagent in a 96-well plate. After 30 min of incubation at room temperature, the reaction was stopped by the LDH stop solution. Then the absorbance was measured at 490 and 680 nm using a microplate reader (Cytation 5, BioTek, Winooski, VT, USA). The cytotoxicity level was calculated by subtracting the absorbance at 680 nm from the absorbance at 490 nm.

$$\text{Relative LDH Activity}\ (\%) = \text{A490} - \text{A680}$$

$$\text{Relative LDH Activity} = \frac{\text{Corrected LDH Activityof experimental Group}}{\text{Corrected LDH Activity of Control Group}} \times 100\%$$

2.9. Measurement of Total Antioxidant Capacity (TAC). The antioxidant capacity of U1 macrophages following treatments was assessed using the OxiSelect Total Antioxidant Capacity (TAC) Assay Kit (Cell Biolabs, San Diego, CA, USA). U1 macrophages were treated with a daily dose of 6 μg/mL of DRV or EV-Lip-DRV and cell media were prepared as per the kit instructions. Samples, standards, and controls were added to a 96-well microtiter plate in 20 μL aliquots. Each well then received 180 μL of 1× reaction buffer. After mixing thoroughly, the initial absorbance was measured at 490 nm. The reaction was initiated by adding 50 μL of 1× copper ion reagent

https://doi.org/10.1021/acsanm.4c04637
ACS Appl. Nano Mater. 2025, 8, 6857−6876

to each well and incubating for 5 min on an orbital shaker. The reaction was terminated by adding 50 μL of 1× stop solution, and the final absorbance was measured at 490 nm. Antioxidant capacity was quantified by comparing the net absorbance values (final minus initial) to a standard curve generated from known concentrations of uric acid. Results were expressed as μM copper reduction equivalents (CRE), indicating the total antioxidant capacity of the treated U1 macrophages.

2.10. Determination of HIV p24 by ELISA. The p24 antigen levels in U1 macrophage media were measured by using the HIV p24 Antigen ELISA Kit (Zeptometrix Corporation, Buffalo, NY, USA). U1 cell medium samples were collected, stored at −80 °C, and thawed before analysis. Aliquots of 200 μL of standards, controls, and samples were added to a 96-well ELISA plate and incubated at 37 °C overnight. Wells were washed five times with the wash buffer, followed by the addition of 100 μL of detector antibody solution and another 1-h incubation at 37 °C. After five additional washes, 100 μL of streptavidin-peroxidase working solution was added, and the plate was incubated at 37 °C for 30 min followed by the addition of the substrate solution, and the plate was incubated in the dark at room temperature for 20−30 min. The reaction was stopped by adding 100 μL of stop solution, and absorbance was measured at 450 nm using a cytation 5 cell imaging multi-mode reader (BioTek, VT, USA). p24 concentrations were calculated by comparing absorbance values to a standard curve, with data corrected for any dilution factors, providing an accurate quantification of p24 levels in the samples.

2.11. Measurement of Intracellular Reactive Oxygen Species (ROS). After daily treatment in U1 macrophages, the reactive oxygen species (ROS) levels in treated cells were quantified using flow cytometry with the fluorescent dye CM-H2DCFDA (general oxidative stress indicator, Thermo Fisher Scientific, Waltham, MA, USA). Following treatment, cells were thoroughly washed with PBS to remove any residual treatment compounds. The cells were then resuspended in a solution containing 5 μM CM-H2DCFDA in PBS and incubated in the dark at room temperature for 45 min to allow for dye uptake and conversion. Postincubation, the cells were washed again with PBS to remove excess dye and resuspended in 300 μL of PBS. The fluorescence intensity, corresponding to the ROS levels, was measured using an Agilent NovoCyte flow cytometer, and data acquisition was performed with the instrument's integrated software. This method allowed for the precise detection and quantification of ROS generated from the treated cells.

2.12. Quantification of Cellular Cytokines and Chemokines Level. To measure the protein levels of cytokines and chemokines, we employed the Human Custom ProcartaPlex 9-plex Assay Kit (ThermoFisher Scientific, Waltham, MA, USA). Cell culture supernatant samples were collected and stored at −80 °C until analysis. The assay was conducted following the manufacturer's protocol. Briefly, samples were thawed and centrifuged at 10,000 × g for 5−10 min to remove particulates. The assay plate was prepared by adding 50 μL of magnetic bead solution to each well, followed by washing to remove any unbound beads. Next, 50 μL of standards, controls, and samples were added to the appropriate wells, and the plate was incubated overnight at 4 °C. After incubation, the wells were washed, and 25 μL of detection antibody mixture was added to each well. The plate was incubated with shaking at room temperature for 30 min and washed again, and then 50 μL of SAPE solution was added. Following a final incubation and wash, 120 μL of reading buffer was added to each well. The plate was then read using a Luminex instrument to quantify the levels of each target protein.

2.13. Measurement of Intracellular DRV Concentrations. For intracellular DRV estimation, U1 macrophages were treated with 6 μg/mL DRV/EV-Lip-DRV for 0.15, 0.5, 1, 4, 10, 24, 48, and 72 h. Cells were harvested in RIPA and were subjected to LC-MS/MS for DRV amount estimation following the method we published earlier.[19]

2.14. In Vitro Hemocompatibility. Red blood cells (RBCs) were isolated from a blood sample acquired from the Interstate Blood Bank Inc. (Memphis, TN). This sample was collected from deidentified human donors with the approval of the Institutional Review Board at the University of Tennessee Health Science Center (UTHSC). Modifications were made to an existing protocol to conduct the hemolysis assay.[21] A suspension of 13.5 million RBCs in 300 μL of PBS was incubated with DRV or EV-Lip-DRV formulation at concentrations of 6, 24, 60, and 120 μg/mL. This incubation was carried out for 2 h at 37 °C. PBS served as the negative control, while deionized water (dH_2O) was used as the positive control. Following the incubation, the suspension was centrifuged at 1000 × g for 10 min at 4 °C. From this, 200 μL of the supernatant was transferred to a 96-well plate to measure the absorbance at 570 nm. The supernatant was also diluted 50× in PBS to be imaged on the glass slide using an Olympus IX73 inverted microscope (Evident Scientific, Inc., Waltham, MA, USA). The percentage of hemolysis was calculated using the following equation:

$$\text{Hemolysis (\%)} = \frac{[\text{ODtest}] - [\text{ODneg}]}{[\text{ODpos}] - [\text{ODneg}]} \times 100\%$$

2.15. Drug Delivery to Mice Brain. 10- to 12-week-old male and female C57BL/6 mice were obtained from Jackson Laboratory (Bar Harbor, MA). Upon arrival, the mice were acclimated to the animal facility for a minimum of 7 days. The animals were housed in groups of five per cage in a sterile room with a 12-h light/dark cycle. The room temperature and humidity were consistently regulated. Food and water were provided ad libitum. Animal studies were conducted under the protocol approved by the Institutional Animal Care and Use Committee (IACUC) at UTHSC. For the investigation of the permeability of EV-Lip-DRV, we dosed the DRV or EV-Lip-DRV via intraperitoneal (IP) and intranasal (IN) routes. For IN, the maximum volume we used for one nostril is 100 μL. (n = 5, IP: 5 mg/kg, IN: 2.5 mg/kg) DRV for the free drug group was prepared in 5% DMSO, 80% PEG400, and 15% PBS as published earlier.[20] We collected the brain, lungs, and liver at 3 h after administration. Due to the limited volume that we can dose via the IN route, we dosed mice with a 30 min gap with a maximum volume of 50 μL at a time. The organs were homogenized and subjected to drug estimation using the LC-MS/MS method we published earlier.[19,20]

2.16. Infection of EcoHIV in Mice. We used the chimeric HIV, EcoHIV-NDK, to infect the C57BL/6J mice following the protocol published by Alfar et al.[22] EcoHIV-NDK plasmid was acquired from Dr. David J. Volsky' lab at the School of Medicine at Mount Sinai. Briefly, EcoHIV-NDK virus stocks were generated by transfecting plasmid DNA into the 293T cells. The cell media was collected, and the virus amount was determined by the p24 level following the aforementioned ELISA method. The virus stock was stored at −80 °C and resuspended in saline for retro-orbital injection. Each mouse was injected with 8.4 μg of virus as of the p24 level. After 21 days of EcoHIV infection, 2.5 mg/kg of DRV or EV-Lip-DRV were administered to mice daily via IN or IP routes. Behavioral studies were conducted on days 20 and 31. Mice were euthanized on day 31 and brains were collected for further pathological analysis.

2.17. Novel Object Recognition (NOR) Test. The NOR test was conducted following the published method.[23] During the training session, mice were habituated to an empty arena, consisting of a standard-size box (45 cm × 45 cm × 35 cm), for 10 min each day over 5 consecutive days. In the testing session, each mouse was presented with two identical objects during the first session for 10 min. After the sample object exposure, the animal was returned to its home cage for a 1-h retention period. In a second session, one of the objects was replaced with a new object for 5 min. The amount of time that the mice spent exploring the new object served as an index of recognition memory. The arena and objects were cleaned with 70% ethanol after each session. All trials were recorded and video tracked using the EthoVision XT 7 automated tracking system (Noldus, Leesburg, VA, USA).

The software computed the time spent exploring each object during the test sessions. These data were then used to determine the recognition index (RI), and discrimination index (DI) calculated with the following equations:

https://doi.org/10.1021/acsanm.4c04637
ACS Appl. Nano Mater. 2025, 8, 6857−6876

$$\text{Discrimination index (DI)} = \frac{\text{Novel Object Exploration - Familiar Object Exploration Time}}{\text{Total Exploration Time}}$$

$$\text{Recognition index (RI)} = \frac{\text{Novel Object Exploration Time}}{\text{Total Exploration Time}}$$

2.18. CatWalk XT Gait Analysis. The CatWalk test for gait analysis was conducted using the CatWalk XT automated analysis apparatus (Noldus Information Technology, Wageningen, The Netherlands) on day 31. A detailed description of the gait analysis has been previously published.[24] In brief, the mice were trained to cross the walkway for 30−45 min each day over six consecutive days before establishing the baseline. The CatWalk system consists of a glass-surfaced walkway illuminated with green light from below and a red light source from above. The CatWalk XT system captures images of the animal's footprints and foot force profiles as they cross the illuminated glass plate. The green light highlights the paw prints, while the red light provides contrast for the animal's body contours, recorded by an automated camera below the glass plate. On the final day of the experiment, each animal underwent three trials, and the mean values from these trials were used for the final analysis.

2.19. Western Blot. We assessed the protein expression related to inflammatory cytokines and chemokines, oxidative stress markers, and neuronal damage markers in the control and EcoHIV mouse brains using Western blotting. The mice brain samples were homogenized in 3 times the volume of PBS. For BCA analysis, brain homogenates were diluted in 2 times the volume of RIPA. After 10−15 min incubation on ice, samples were subjected to 10,000 × *g* centrifugation for 5 min. The supernatant was collected and diluted 6 times in RIPA for the measurement of the protein concentration of the brain samples.

We evaluated the protein expression of inflammatory cytokines and chemokines, oxidative stress markers, and neuronal damage markers in control and EcoHIV mouse brains using Western blotting. Mouse brain samples were homogenized in three volumes of PBS. For BCA analysis, brain homogenates were diluted with two volumes of RIPA buffer. After incubating on ice for 10−15 min, the samples were centrifuged at 10,000 × *g* for 5 min. The supernatant was collected and diluted 6-fold in RIPA buffer to measure the protein concentration using the Pierce BCA Protein Assay Kit (23225, Thermo Scientific, Waltham, MA, USA).

We assessed the expression of inflammatory cytokines and chemokines, including IL-6, IL-1β, MCP-1, and IL-18, along with oxidative stress markers superoxide dismutase 1 (SOD1) and catalase. Neural marker proteins NeuN, IBA1, synaptophysin, and TMEM119 were used to evaluate neural damage. All protein expression levels were normalized to that of β-actin. Equal amounts of protein (12 μg) from control, HIV without treatment, and HIV treated with DRV and EV-Lip-DRV mouse brain homogenates were used. Proteins were separated on a polyacrylamide gel with a 4% stacking gel and a 10% resolving gel. Electrophoresis was conducted at 60 V for 50 min, followed by 150 V for another 50 min. Proteins were then transferred to a polyvinylidene fluoride (PVDF) membrane at 0.35 Amp for 90 min. Following the transfer, the membrane was incubated with 5−10 mL of Li-Cor blocking buffer (LI-COR Biosciences, Lincoln, NE, USA) for 1 h to minimize nonspecific antibody binding. The membrane was then incubated overnight at 4 °C with primary antibodies specific to the target proteins. The detailed information on the primary antibodies used in this study was summarized in Table 1.

The next day, the blots were washed three times with 0.2% Tween-20 PBST solution and then incubated with the appropriate secondary antibodies—Goat anti-Mouse Mab (1:10,000 dilution, LI-COR Biosciences) and Goat anti-Rabbit Mab (1:10,000 dilution, LI-COR Biosciences)—for 1 h at room temperature in the dark. After an additional round of washing with PBST, the membranes were scanned using Image Studio Lite version 4.0 on a Li-Cor Scanner (LI-COR Biosciences). LI-COR Image Studio Lite version 4.0. (Nebraska, USA) software was used to perform the densitometry analyses of the proteins, with β-actin serving as an internal loading control to normalize protein expression levels.

Table 1. List of the Detailed Information on the Primary Antibodies

Antibody	Species	Dilution factor	Product information
β-actin	mouse	10,000	Proteintech, 66009-1-Ig
IL-6	rabbit	1000	Proteintech, 21865-1-AP
IL-1β	rabbit	1000	Proteintech, 26048-1-AP
MCP-1	mouse	500	Proteintech, 66272-1-Ig
IL-18	rabbit	1000	Proteintech, 10663-1-AP
SOD1	mouse	500	Santa Cruz Biotechnology, sc-101523
Catalase	mouse	1000	Santa Cruz Biotechnology, sc-365738
NeuN	rabbit	1000	Proteintech 26975-1-AP
IBA1	rabbit	500	Proteintech, 10904-1-AP
Synaptophysin	mouse	2000	Proteintech, 67864-1-1g
TMEM119	rabbit	500	Proteintech, 27585-1-AP

2.20. DNA Damage in the Brain. DNA was isolated from 100 μL of brain homogenates using the QIAamp DNA Mini Kit (QIAGEN, Germantown, MD, USA) following the manufacturer's protocol. DNA concentrations were determined by measuring the absorbance of 1 μL of the sample at 260/280 nm with a NanoDrop 2000 spectrophotometer (Thermo Scientific, Waltham, MA, USA)

3. RESULTS AND DISCUSSION

3.1. Development and Characterization of EV-Lip-DRV Formulation. A schematic representation of the preparation of EV-Liposome-DRV (EV-Lip-DRV) is illustrated in Figure 2A. This process involves the use of EV from healthy mouse plasma, followed by thin film hydration to incorporate DRV into liposomes, sonication of the EV and liposomes, and extrusion, resulting in the EV-Lip-DRV formulation. The free DRV or unloaded DRV was removed from the formulation by ultrafiltration. We optimized the ratio of the lipids and drug based on the work published earlier[12] to ensure the adequate concentration of DRV in the formulation to proceed with the animal studies. The encapsulation efficiency percent (EE%) of the formulation from 8 preparations was 41.75 ± 2.19%.

Transmission electron microscope (TEM) images in Figure 2B reveal the morphological characteristics of EVs and EV-Lip-DRV. The EVs displayed a size of approximately 93.3 nm, while the EV-Lip-DRV exhibited a slightly reduced size of 85.3 nm. The size and zeta potential of the EV, EV-Lip, and EV-Lip-DRV formulations were measured and compared (Figure 2C). The average size of the EVs was found to be 142.90 ± 5.26 nm, with a zeta potential of −12.47 ± 0.38 mV. In contrast, the EV-Lip formulation exhibited an increased size of 186.60 ± 0.67 nm and a reduced zeta potential of −4.40 ± 0.38 mV. The EV-Lip-DRV formulation showed a similar size to EV-Lip at 189.10 ± 2.42 nm and a zeta potential of −7.76 ± 0.41 mV. These results indicate that the encapsulation of DRV during the fusion of EVs and liposome membranes led to a slight increase in particle size and a modification in surface charge. We measured the changes in size on days 29, 37, 45, 50, and 78 following the isolation of EVs or the preparation of EV-Lip-DRV (Figure 2D). The size of EVs changed significantly after 45 days at room temperature and increased markedly after 78 days when stored at 4 °C. In contrast, the EV-Lip-DRV maintained its size consistently over 78 days, regardless of the storage conditions. Western blot analysis, as shown in Figure 2E, confirms the presence of EV markers CD63, Alix, and CD9

https://doi.org/10.1021/acsanm.4c04637
ACS Appl. Nano Mater. 2025, 8, 6857−6876

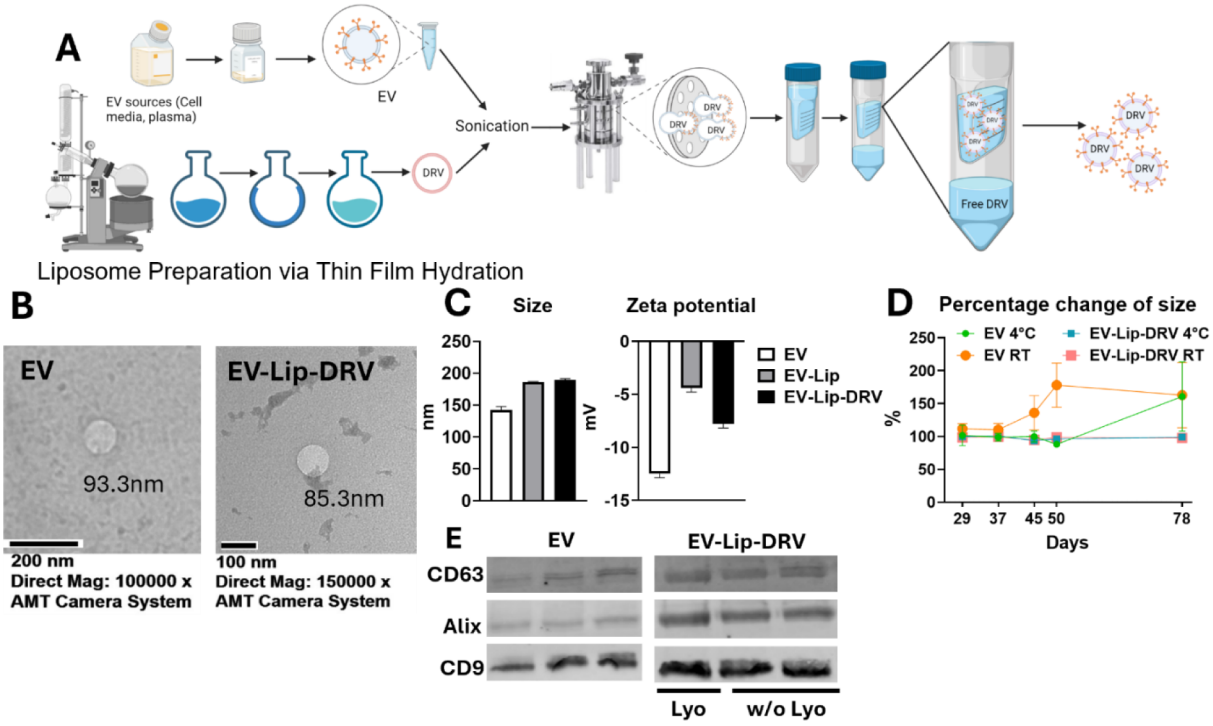

Figure 2. A. Schematic diagram of the preparation of the EV-Liposome-DRV (EV-Lip-DRV) formulation and hypothetical structure of EV-Lip-DRV. This diagram shows the process used to create EV-Lip hybrid systems for drug loading. The process involves integrating liposome phospholipids, EV phospholipids, cholesterol, EV membrane markers, and the drug to form the EV-Lip hybrid. The encapsulation efficiency percent (EE%) of EV-Lip-DRV is 41.75 ± 2.19%. B. Transmission electron microscope (TEM) image of EVs and EV-Lip-DRV. C. Size and zeta potential of EV and EV-Lip-DRV. EV: 142.90 ± 5.26 nm, −12.47 ± 0.38 mV; EV-Lip: 186.60 ± 0.67 nm, −4.40 ± 0.38 mV; EV-Lip-DRV: 189.10 ± 2.42 nm, −7.76 ± 0.41 mV. D. Percentage of size change 29, 37, 45, 50, 78 days storage at room temperature and 4 °C after preparation (n = 3). E. Western blot of EV and EV-Lip-DRV from three different batches. The mean ± SEM provided is from n = 4.

in both EVs and EV-Lip-DRV. The consistency of marker expression across three different batches demonstrates the reproducibility of the formulation process. The retention of plasma EV-specific markers on EV-Lip-DRV membranes enhances the potential for effective drug delivery to the brain by improving targeting, biocompatibility, stability, cellular uptake, and controlled release of the drug.

Delivering ART drugs to the brain is particularly challenging due to the restrictive nature of the BBB, which results in subtherapeutic drug concentrations within the CNS, enabling HIV persistence.[18] Consequently, advanced delivery systems are imperative to facilitate the efficient translocation of ART drugs across the BBB for optimal therapeutic efficacy.

We fused EVs with drug-loaded liposomes, utilizing the advantages of both systems through a thin film process, followed by extrusion. EVs offer high biocompatibility and the ability to target specific cells due to their natural origin, enhancing the delivery of therapeutic agents to desired tissues,[25] which has the potential for drug delivery in the brain.[7,26] Liposomes, on the other hand, provide excellent drug encapsulation efficiency and the capability to protect drugs from degradation and deliver the drugs across the BBB, ensuring sustained release and stability.[27] However, using EVs alone can be challenging due to their limited drug loading capacity and potential variability in isolation methods.[25,26] Similarly, liposomes alone may suffer from rapid clearance by the reticuloendothelial system and potential immunogenicity, which can limit their efficacy and safety.[28] To achieve optimal fusion with plasma-derived extracellular vesicles, we selected 1,2-dioleoyl-*sn*-glycero-3-phosphocholine (DOPC) and cholesterol as the primary lipid components, given their abundant presence in EV membranes.[13] On the other hand, the transition/melting temperature of DOPC is −17 °C, which allows its phase to be maintained under a liquid crystalline phase at room temperature without additional temperature control for the extruder. There are various techniques to fuse the membranes of EV with liposomes.[8,29] Extrusion was chosen for its efficiency and cost-effectiveness in scale-up. We sourced EVs from healthy mice plasma, and healthy human plasma, selecting based on the intended application: mice plasma-derived EVs for mice studies and human plasma-derived EVs for physicochemical characterization, U1 treatment, and hemolysis studies. This strategy enhances the applicability of EV-Lip nanoparticles for personalized medicine.

EVs were isolated using a commercial kit to ensure sufficient yield within a short time frame with sufficient quality and quantity for drug formulation. We chose to use the commercial kit to isolate the EVs because we can get a sufficient EV amount with reasonable quality for each formulation preparation from 0.5 to 1 mL of plasma samples. Our previous trials on loading drugs in EVs using the sonication and freeze−thaw method did not produce EE% higher than 12%, which is not sufficient for treatment in vitro and in vivo systems. The EE% of DRV in EV-Lip hybrid nanoparticles in this study was improved to 41.75%, though it is lower compared to the 84.19% EE% in PLGA DRV nanoparticles.[19] The EE% of EV-Lip hybrid nanoparticles can vary widely, ranging from 15% to 90%, depending on factors such as loading methods, lipid composition, liposome/EV ratio, the physicochemical proper-

https://doi.org/10.1021/acsanm.4c04637
ACS Appl. Nano Mater. 2025, 8, 6857−6876

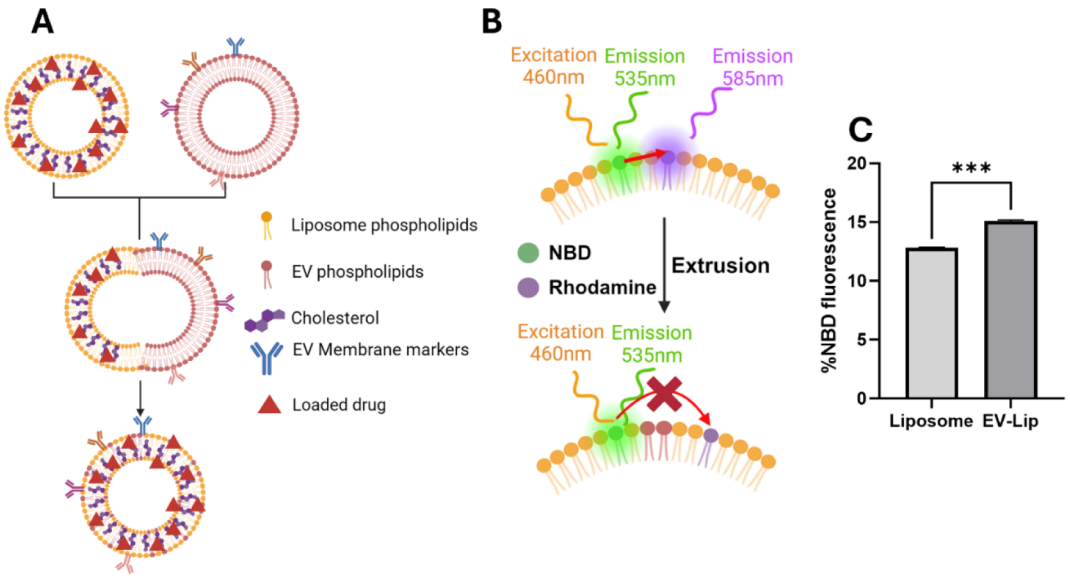

Figure 3. A. Schematic description of the process to produce EV-Lip hybrid to load drug. B. Schematic illustration of fluorescence resonance energy transfer (FRET) membrane fusion analysis using fluorophores, rhodamine, and NBD. When lipid fusion takes place, the NBD signal increases due to the greater distance between the two probes. The FRET assay is highly sensitive to changes in the distance between fluorophores, making it an excellent tool for studying the dynamics of membrane fusion in real-time. In this study, two fluorophores were located on liposome membranes. As membranes of EV and liposomes fuse, donor (NBD) and acceptor (rhodamine) fluorophores come further from each other. When NBD was excited at 460 nm, it emitted light at 535 nm, which in turn excited the nearby rhodamine. C. Percentage of NBD fluorescence intensity increased in the EV-Lip hybrid, indicating the membrane fusion of the liposome and EV-Lip.

ties of the drug molecule, and the purification method used to remove unloaded drugs.[30−32] For example, the doxorubicin has been loaded in different EV-Lip hybrid nanoparticles with EE% from 30 to 88%.[31,33] The formulation with high EE% involves the step dissolving the EV in methanol: chloroform (1:1) and mixing with the mixed lipids solution in chloroform.[33] It should be mentioned that even though EV was dissolved in the organic solvent, the EV membrane marker protein, CD63, was still detected in these hybrid nanoparticles. However, when the fusion of EV and liposome was conducted in PBS, the EE% was 30%.[31] The preparation process can be modified without degrading the biomarker on the EV membrane to further optimize our formulation and improve the EE%.[30,31]

The sizes of EV-Lip nanoparticles with and without DRV loaded were larger compared to EV. Upon fusion with liposomes, the absolute value of surface charge indicated by the zeta potential was decreased. FRET analysis confirmed the membrane fusion between the EV and liposome. The integrity of the vesicle upon fusion was maintained as evidenced by TEM. We further confirmed that the membrane proteins, such as CD63, Alix, and CD9 presented on the EV membrane, were retained in the EV-Lip hybrid nanoparticles. The change of size in the nanoparticle over the period of storage may indicate the aggregation of the nanoparticle, which suggests a decrease in its stability. EV-Lip-DRV formulation exhibited exceptional stability over time, maintaining consistent size for 78 days under both room temperature and 4 °C storage conditions. In contrast, EVs alone showed significant size changes after 45 days at room temperature and a notable increase after 78 days at 4 °C, indicating their relative instability. Studies have shown that the storage of mouse bronchoalveolar lavage fluid (BALF) EV at 4 °C for 4 days results in 10% of increase in size.[34] This suggests that the fusion with liposomes and incorporation of DRV significantly enhance the structural stability of EVs. This aligns with previous research findings that the hybrid nanoparticles are stable at 4 °C at least 4 weeks.[35,36] Rayamajhi et al. developed a macrophage-derived exosome-liposome hybrid nanoparticle loaded with doxorubicin for targeted drug delivery to tumor.[36] The hybrid nanoparticles exhibited superior stability over 30 days compared to exosomes, which demonstrated significant size changes over time. The doxorubicin-loaded EV-Lip nanoparticles developed by Barbosa et al. also showed good long-term storage stability under 4 °C for 90 days.[33] Kim et al. also demonstrated that all their doxorubicin-loaded EV-Lip formulations maintain size stability in saline and 10% FBS over 4 weeks at 4 °C and for 24 h at 37 °C. Additionally, two of their EV-Lip formulations remained stable even in the presence of the surfactant Triton X-100.[37] Quantification of the number of nanoparticles is also an emerging method to determine the stability of the nanoparticles; however, the results of some studies showed inconsistent conclusions. A study examining exosomes collected from HEK293 cells found that storage at 4 or 37 °C for 24 h resulted in higher particle numbers compared to storage at −80 °C.[37] Another study using the EV from neutrophilic granulocytes showed a significant decrease in EV number after storage at 4 and 20 °C in 1 day compared to storage at −20 °C.[38] These conflicting findings highlight the complexity of EV storage and the need for careful consideration of storage conditions based on the specific EV source and experimental requirements. To minimize the influence of stability on the effects of DRV-EV-Lip in both in vitro and in vivo experiments, all formulations in this study were utilized within 24 h of preparation. In future studies, we will evaluate the optimal long-term storage conditions for our hybrid system.

The stability of EVs and liposomes is a significant concern for their clinical application, particularly when nucleotides or proteins are present in the particles. For example, COVID-19 liposome-based mRNA vaccines require long-term storage in

https://doi.org/10.1021/acsanm.4c04637
ACS Appl. Nano Mater. 2025, 8, 6857−6876

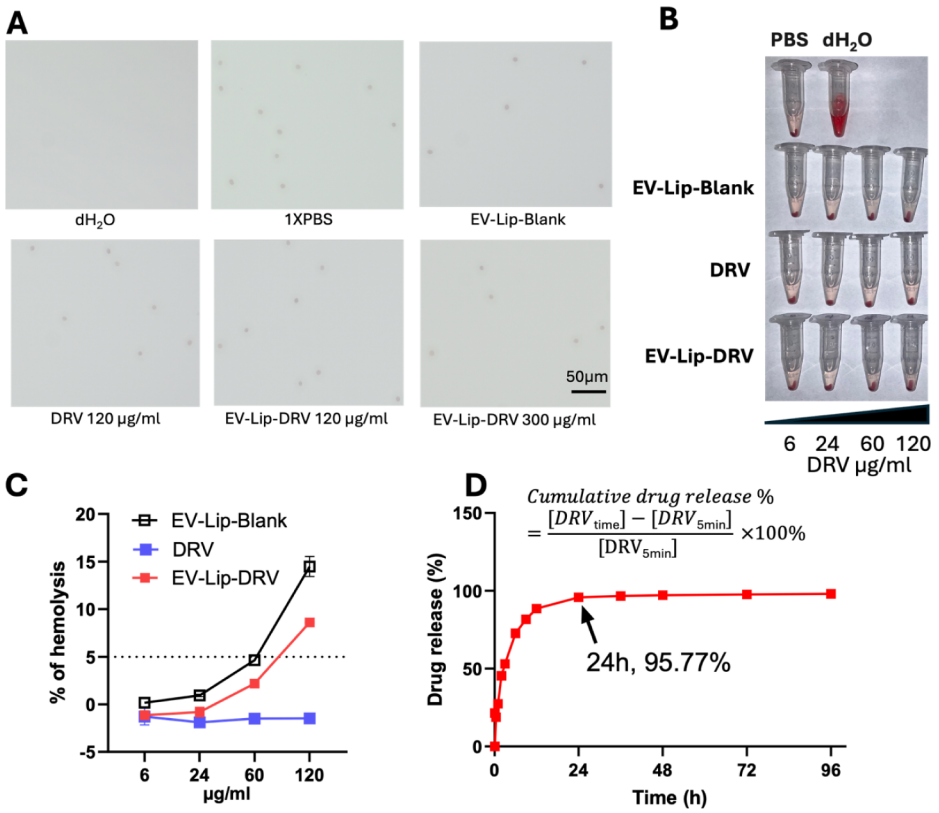

Figure 4. In vitro hemocompatibility and drug release profile of EV-Lip-DRV. A. Microscopic view of human red blood cells under exposure to dH_2O, PBS, EV-Lip, DRV, and EV-Lip-DRV at indicated concentrations. B. Visual inspection of RBCs after incubating with indicated solutions at 37 °C for 2 h. C. Ratio of hemolysis of RBCs with exposure to EV-Lip-DRV formulations at the indicated concentrations. D. In vitro drug release profile. The cumulative drug release was measured at 5 min, 15 min, 30 min, 1 h, 2 h, 3 h, 6 h, 9 h, 12 h, 24 h, 36 h, 48 h, 72 h, 96 h. At 24 h, 95.77% of DRV was released from the EV-Lip formulation.

the freezer at −50 to −15 °C for Moderna's SPIKEVAX vaccine[39] and −90 to −60 °C for Pfizer/BioNTech's COMIRNATY vaccine,[40] which was a big challenge for the supply chain to maintain a shelf life of 18 months. Despite this challenge, the development and application of liposome formulations have continued to progress. Lyophilization is a technique widely used to increase the shelf life of liposome formulation shelf life. From our results, lyophilization did not affect the EV proteins. However, our EV-Lip nanoparticles were prepared in PBS, which will cause crystallization and a pronounced shift of pH during the lyophilization process and is not ideal for the EV-Lip nanoparticles to retain their integrity and biological function during lyophilization. So further efforts need to be made to optimize the lyophilization of the EV-Lip formulation as this is very critical for the long-term storage of the EV-Lip formulation for clinical use. Therefore, the EV-Lip formulation still has the potential to be applied as an ideal target drug delivery system.

3.2. Proof of Membrane Fusion. The membrane fusion between EVs and liposomes (Figure 3) was analyzed using FRET, as depicted in Figure 3B. As shown in Figure 3A, in liposomes alone, rhodamine quenched the nitrobenzoxadiazole (NBD) fluorescence. However, upon membrane fusion between EV and lipid membranes, there was an increase in NBD fluorescence. Although we could not quantify the exact percentage of membrane fusion based on FRET, a significant increase in the percentage of NBD fluorescence based on total absorbance at 585 and 535 nm suggests successful membrane fusion (Figure 3C). The change in the percentage of NBD fluorescence varied across the studies.[10,41] Piffox et al. showed 8−15% change in NBD fluorescence when increasing the percentage of polyethylene glycol (PEG) used in the formulation, which indicated that the EV source and ratios of synthetic components in the hybrid system play a role in fusion efficiency.[41] In the future, the fusion efficiency can be optimized as needed.

3.3. Hemocompatibility and Drug Release Profile of EV-Lip-DRV. Figure 4A presents microscopic images of human RBCs exposed to various solutions (dH_2O, PBS, EV-Lip-Blank, DRV at 120 μg/mL, EV-Lip-DRV at 120 μg/mL, and EV-Lip-DRV at 300 μg/mL) following a 2-h incubation at 37 °C. The images show that RBCs exposed to EV-Lip-DRV formulations maintained their morphology without significant changes compared to the control groups, indicating good hemocompatibility. Visual inspection of RBCs in Figure 4B corroborates these findings, with RBCs treated with dH_2O (positive control) displaying significant hemolysis, as evidenced by the red coloration, whereas EV-Lip-DRV formulations caused minimal hemolysis, comparable to that of the PBS and EV-Lip-Blank controls. Further quantification in Figure 4C shows the hemolysis percentage for RBCs exposed to different concentrations (6, 24, 60, 120 μg/mL) of EV-Lip-Blank, DRV, and EV-Lip-DRV, revealing that the hemolysis percentage for EV-Lip-DRV remained consistently below 15%, which is within the acceptable range for hemocompatibility. This confirms that the EV-Lip-DRV formulations are safe for RBCs. The microscopic images, visual inspection images, and hemolysis data indicate that EV-Lip-DRV formulations exhibit

https://doi.org/10.1021/acsanm.4c04637
ACS Appl. Nano Mater. 2025, 8, 6857−6876

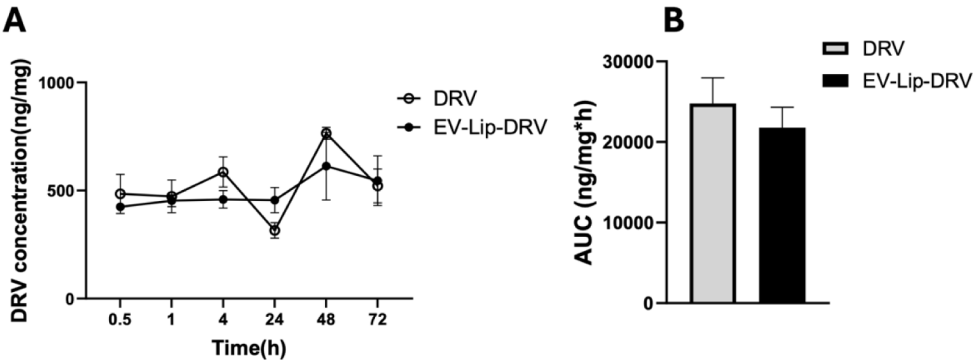

Figure 5. U1 monocytes were differentiated into macrophages upon treating 100 nM PMA for 72 h followed by treatment of 6 μg/mL DRV, EV-Lip-DRV for 0.15, 0.5, 1, 4, 10, 24, 48, and 72 h. A. DRV concentration for up to 72 h was measured by LC-MS and normalized by cellular protein level. B. Area under the curve (AUC) was estimated based on the DRV concentrations. DRV concentration was normalized using per mg of protein in cell extract (mean ± SEM, n = 4).

good hemocompatibility. Though we are moving forward to IN routes, the percentage of hemolysis remains relatively low across different concentrations (6, 24, and 60 μg/mL), suggesting that the formulation is safe for even intravenous administration.

Figure 4D presents the cumulative drug release profile of DRV from the EV-Lip formulation. The release was monitored at various time points (5 min, 15 min, 30 min, 1 h, 2 h, 3 h, 6 h, 9 h, 12 h, 24 h, 36 h, 48 h, 72 h, 96 h). The results showed that 95.77% of DRV was released from the EV-Lip formulation within 24 h, demonstrating a sustained release profile. The cumulative drug release profile showed an extended release for 48 h. This suggests that the formulation is efficient in delivering the drug in an extended-release manner, which is critical for therapeutic efficacy. EV-Lip nanoparticles have shown extended-release profiles in other studies. For example, the EV-Lip-Paclitaxel nanoparticle releases 95% of the loaded drug in 20 h with a sustained release profile over 48 h.[42] EV-Lip-doxorubicin with the same lipid component fabricated with EVs from different breast cancer cells exhibits varying drug release profiles.[33,43] One study reported that 96.6% of doxorubicin is released within 24 h at pH 5.0, compared to 70.1% at pH 7.4, demonstrating a pH-dependent release mechanism.[43] Conversely, another study observed a slower and more sustained release, with 51.8% of doxorubicin released at pH 5.0 and 29.2% at pH 7.4 over the same time span.[33] These findings underscore the impact of modifying the components of the hybrid nanoparticle system on the drug release profile and highlight the influence of pH on drug release kinetics. Such modifications can be strategically employed to tailor the EV-Lip nanoparticle system for specific therapeutic needs, optimizing the release rate for extended or controlled delivery.

3.4. Effective Uptake of EV-Lip-DRV in Differentiated Macrophages. As shown in Figure 5, the concentration of DRV in U1 macrophages was measured at indicated time points using LC-MS, and the data were used to calculate the area under the curve (AUC). The results showed that DRV and EV-Lip-DRV have similar drug concentration profiles over time, with no significant differences observed in the AUC between the two groups. This suggests that the encapsulation of DRV in EV-Lip does not adversely affect the drug's uptake and retention in macrophages. The comparable AUC values further confirm the delivery and retention of DRV from the EV-Lip-DRV formulation in U1 macrophages.

The exceptional phagocytic ability of U1 macrophages plays an important role in the cellular uptake of nanoparticles, which may overshadow the influence of EV-Lip particles. Technically, the target delivery characteristic of EV will endow the same property on EV-Lip nanoparticles; however, the cellular uptake of EV-Lip nanoparticles did not consistently show improvement across different studies.[33,35] The cellular uptake of the drug in the hybrid nanoparticle can vary with certain EV: lipid ratios, as indicated by the protein of EV and weight of lipids. Kim et al. demonstrated that cellular uptake of the EV-Lip-doxorubicin hybrid nanoparticles with EV:lipid ratios of 1:10, 1:5, and 1:2 did not show any significant differences.[44] Our data suggest that the encapsulation of DRV in EV-Lip with a 1:50 EV:lipid ratio does not negatively impact its uptake and retention in U1 macrophages. In the studies of the EV-Lip-siRNA formulations with EV: lipid ratios of 1:50 and 1:100, Evers et al. proved that the hybrid nanoparticle with 1:50 EV:lipid ratio shows significant improvement in cellular uptake in two of the three cell lines they treated.[45] The observation in our study is consistent with Evers et al. study. The increase of EV does not necessarily ensure advanced cellular uptake, such as the pancreatic cancer cell line-derived EV showed lower cellular uptake compared to its EV-Lip nanoparticle.[31]

In our study, we did not observe a significant improvement in cellular uptake of DRV in the EV-Lip-DRV group in U1 macrophages. However, the relationship between cellular uptake and drug efficacy remains inconsistent across studies, with conflicting results reported in the literature.[33,44,45] Barbosa et al. showed that doxorubicin encapsulated in the EV-Lip increases cellular uptake compared to the liposome formulation in two of the three cancer cell lines.[33] In the study conducted by Barbosa et al., though DOX itself had higher cellular uptake, the EV-Lip-doxorubicin in this study still showed the most significant suppressive effect in the migration test of the three cell lines used in this work.[33] The EV-Lip nanoparticle loaded with clodronate, prepared using a fibroblast cell line (L-929) derived EVs, demonstrated improved cellular uptake in L-929 cells compared to its liposome formulation but not in the macrophage cell line (RAW 264.7). However, the EV-Lip loaded with clodronate showed enhanced therapeutic efficacy for pulmonary fibrosis treatment in a pulmonary fibrosis mice model.[35] Therefore, despite the lack of significant enhancement in cellular uptake of DRV during in vitro treatment, we proceeded with in vivo

https://doi.org/10.1021/acsanm.4c04637
ACS Appl. Nano Mater. 2025, 8, 6857−6876

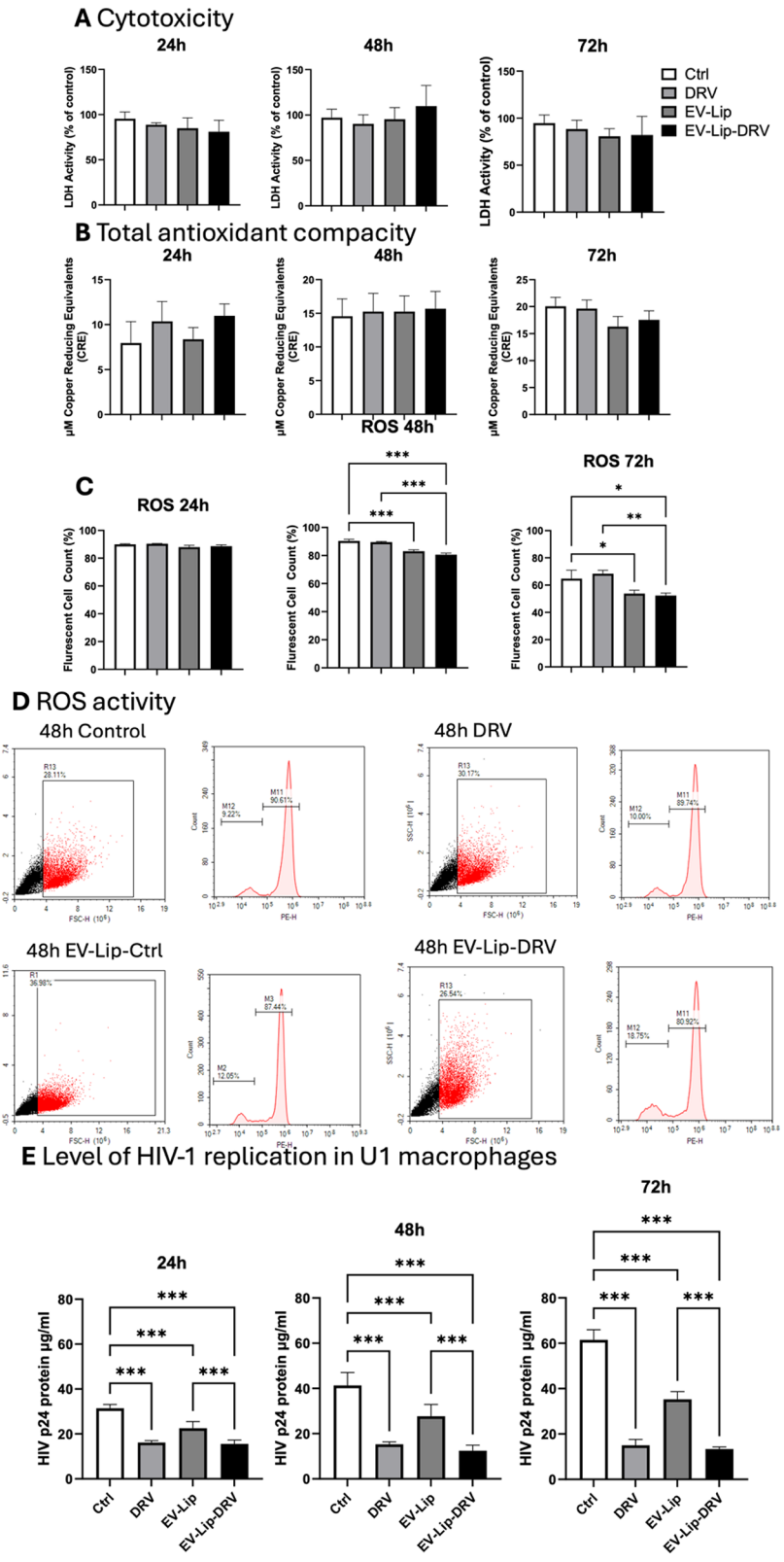

Figure 6. U1 macrophages were treated with 6 μg/mL DRV or EV-Lip-DRV for 24, 48, and 72 h. The control group consists of U1 macrophages cultured under the same conditions but without any treatment. Media was collected for further analysis. A. Cytotoxicity was determined by LDH analysis. B. Total antioxidant capacity indicated by μM of copper reducing equivalents (CRE). C, D. ROS activity measured in the direct treatment of U1 by flow cytometry using CM-DCFDA dye and excitation/emission at 495/519 nm. Data are quantified using fluorescent cell count that was measured in %. E. HIV p24 protein level in U1 macrophage culture media was measured to indicate the level of HIV-1 replication after exposure to 6 μg/mL DRV/EV-Lip-DRV for 24, 48, and 72 h. p24 level in U1 media was measured. The group without treatment was indicated as control group. Statistical analyses were carried out by using ANOVA. Results are expressed as means ± SEM of $n = 3$. *$p < 0.05$, **$p < 0.01$, ***$p < 0.001$.

https://doi.org/10.1021/acsanm.4c04637
ACS Appl. Nano Mater. 2025, 8, 6857−6876

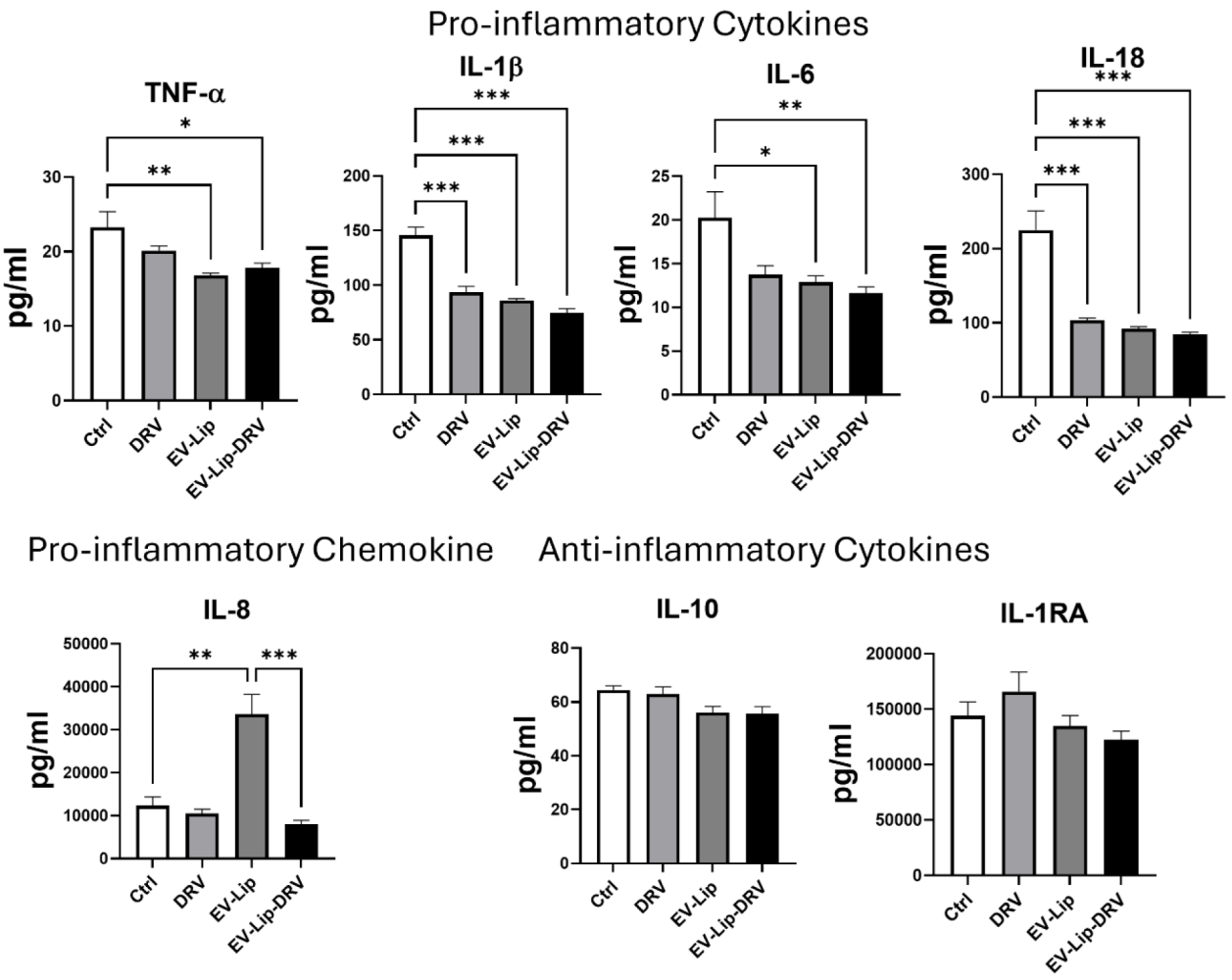

Figure 7. Multiplex ELISA of cytokines and chemokines assay in U1 macrophages upon exposure to DRV, EV-Lip, and EV-Lip-DRV for 48 h. Results are obtained from 6 samples, expressed as means ± SEM. One-way ANOVA test was used for data analysis; * $p < 0.05$, ** $p < 0.01$, *** $p < 0.001$.

studies to assess the effectiveness of the EV-Lip hybrid system for brain drug delivery in animal models.

In this study, we have not examined the mechanism of cellular uptake of EV-Lip-DRV. We are aware that several factors contribute to the cellular uptake of the nanoparticle, and we will explore the mechanism in our future studies. The specific interactions between different cells and various hybrid nanoparticles are still not well understood, necessitating cellular uptake tests on the target cells during the development and optimization of the hybrid nanoparticle. However, cellular uptake should not be the limiting factor during the screening process, and pharmacological studies still need to be performed both *in vitro* and *in vivo* to further confirm the effects of the hybrid nanoparticle on macrophage effector functions.

3.5. Effect of EV-Lip-DRV on Cytotoxicity, Antioxidant Capacity, and Reactive Oxygen Species (ROS) Activity in U1 Macrophages. As shown in Figure 6A, lactate dehydrogenase (LDH) activity was measured to assess the cytotoxicity. There were no significant differences in LDH activity across all groups (Ctrl, DRV, EV-Lip, EV-Lip-DRV) at 24, 48, and 72 h, indicating that the treatments did not induce cytotoxicity.

Figure 6B presents the total antioxidant capacity of the cells measured in micromolar copper-reducing equivalents (CRE). The antioxidant capacity remained stable across all treatment groups at 24, 48, and 72 h, suggesting that neither DRV nor EV-Lip-DRV treatments adversely affected the cells' antioxidant defenses.

Figure 6C,D shows the measurement of ROS activity through flow cytometry using CM-DCFDA dye. At 24 h, there was no significant difference in ROS levels among the groups. However, at 48 h, the fluorescent cell count, indicative of ROS activity, showed a significant reduction in the EV-Lip groups compared to the HIV control group (***$p < 0.001$). At 72 h, ROS levels significantly decreased in both the EV-Lip and EV-Lip-DRV treatment groups compared to the HIV control group (*$p < 0.05$, **$p < 0.01$, ***$p < 0.001$). Specifically, the EV-Lip-DRV group maintained a higher fluorescent cell count, aligning with the quantified ROS data. This indicates that the effect of the EV-Lip treatments was sustained throughout the 72-h period.

Overall, the results demonstrated that DRV and EV-Lip-DRV treatments do not induce cytotoxicity or significantly alter the antioxidant capacity in U1 macrophages. However, ROS activity was modulated over time, with significant reductions observed at 48 and 72 h, particularly in the DRV and EV-Lip groups. This suggests that while the EV-Lip-DRV formulation is effective in reducing oxidative stress, it maintains better ROS stability over time compared to that of DRV and EV-Lip alone.

https://doi.org/10.1021/acsanm.4c04637
ACS Appl. Nano Mater. 2025, 8, 6857−6876

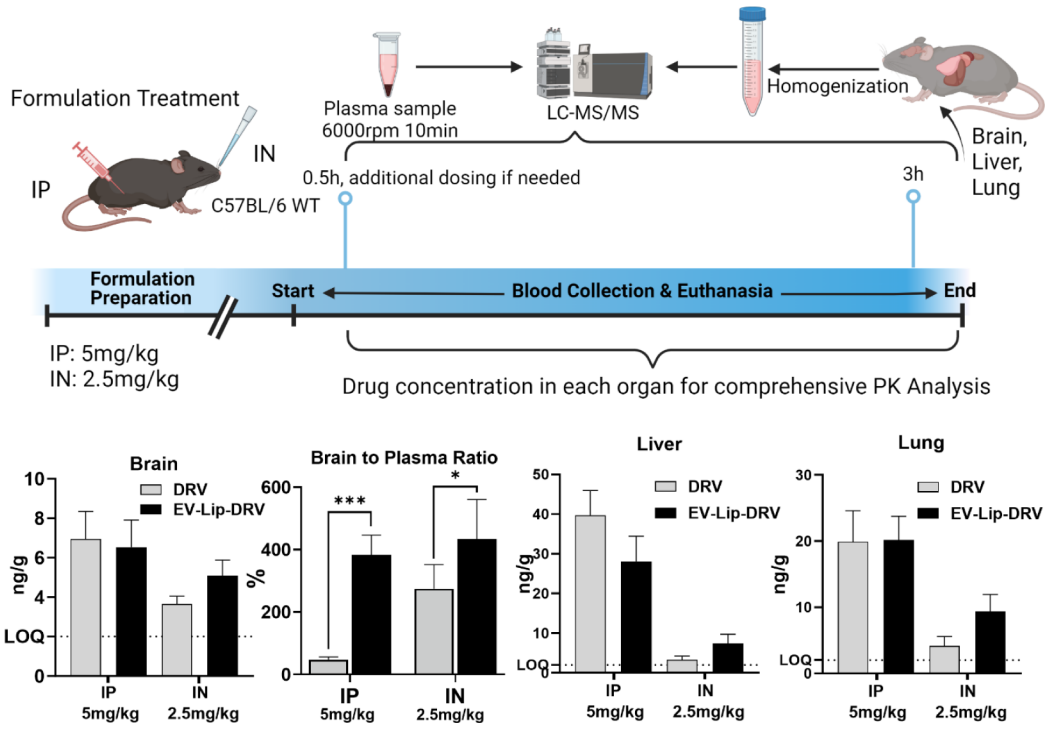

Figure 8. Biodistribution of 5 mg/kg DRV administered via intraperitoneal (IP) and 2.5 mg/kg DRV using intranasal (IN) in C57BL/6 wild-type mice. DRV concentration was determined in mice's brains, plasma, lungs, and liver after administration of DRV or EV-Lip-DRV at 3 h. The brain-to-plasma concentration was calculated by dividing the DRV concentration in the brain by the DRV concentration in the plasma × 100%. The limit of quantification (LOQ) of the LC-MS/MS methods was indicated by the dashed line. Results were expressed as means ± SEM *t* tests were used to compare the differences between two treatment groups; * indicates $p < 0.05$, *** indicates $p < 0.001$, $n = 5$.

3.6. HIV Replication in U1 Macrophages. Figure 6E illustrates the levels of HIV replication in U1 macrophages after 24, 48, and 72 h of exposure to 6 μg/mL DRV or EV-Lip-DRV. HIV replication was assessed by measuring p24 protein levels in the U1 media. At all the time points, both DRV and EV-Lip-DRV significantly reduced p24 levels compared to the control group (***$p < 0.001$). However, compared to DRV alone, there was no further decrease in p24 levels with EV-Lip-DRV treatment. Compared to the control, EV-Lip also showed a decrease in the viral load. These results suggest at least EV-Lip-DRV is as effective as DRV alone in reducing HIV replication in U1 macrophages. Extracellular vesicles (EVs) derived from the semen of healthy volunteers have demonstrated anti-HIV activity by inhibiting the function of intravirion reverse transcriptase.[46] Previous research has demonstrated that EVs derived from HEK293T cells without therapeutic molecules can repress HIV infection in vitro but not in NSG HIV mice.[47] Anionic liposomes, particularly those containing cardiolipin, have demonstrated the ability to inhibit HIV-1 replication in various cell types, including A3.01 and H9 cells by interacting with positively charged regions of the viral envelope proteins during the viral entry process.[48] Given the diverse bioactivities of EVs and liposomes derived from different sources, further research is required to fully understand their potential in anti-HIV activities.

Our study demonstrates that the EV-Lip-DRV formulation significantly inhibits HIV replication in U1 macrophages, as evidenced by the reduction in p24 levels at 24, 48, and 72 h without inducing cytotoxicity and reducing antioxidant capacity.[49] Oxidative stress plays a significant role in HIV pathogenesis, contributing to immune dysfunction and the progression of HAND. HIV gp120, Tat, Nef, and Vpr proteins can induce the production of ROS in microglia and astrocytes.[49,50] The overproduction of ROS and depletion of antioxidants lead to cellular damage and apoptosis in neuronal cells.[50,51] Studies have reported that EVs derived from body fluid or cells of healthy volunteers can reduce oxidative stress[52] and suppress HIV replication.[53] The EV is involved in HIV pathogenesis in the brain, indicating the potential of using EV in the treatment of HAND. This can explain why the EV-Lip itself suppressed HIV replication in U1 cells.

3.7. EV-Lip-DRV Alters HIV-Associated Inflammatory Response. Figure 7 shows the cytokine and chemokine profiles in U1 macrophages treated with DRV, EV-Lip, and EV-Lip-DRV for 48 h, measured using multiplex ELISA. Pro-inflammatory cytokines: TNF-α and IL-6: There was a significant decrease in TNF-α and IL-6 levels in both EV-Lip and EV-Lip-DRV groups compared to the control (*$p < 0.05$, **$p < 0.01$). IL-1β: IL-1β levels were significantly lower in DRV, EV-Lip, and EV-Lip-DRV groups compared to the control (***$p < 0.001$). IL-18: There was a substantial reduction in IL-18 levels in all the groups—DRV, EV-Lip, and EV-Lip-DRV—compared to the control (***$p < 0.001$). Interestingly, EV-Lip also showed a decrease in these proinflammatory cytokine levels. However, there was no further decrease in these proinflammatory cytokines by EV-Lip-DRV compared to DRV or EV-Lip alone. Pro-inflammatory chemokine: IL-8: The level of IL-8 was significantly increased in EV-Lip compared to the control (**$p < 0.01$). However, its level is decreased in EV-Lip-DRV compared to EV-Lip (***$p < 0.001$), suggesting that the EV-Lip-DRV formulation decreases the inflammatory response. Anti-inflammatory Cytokines: IL-10 and IL-1RA: There were no

https://doi.org/10.1021/acsanm.4c04637
ACS Appl. Nano Mater. 2025, 8, 6857−6876

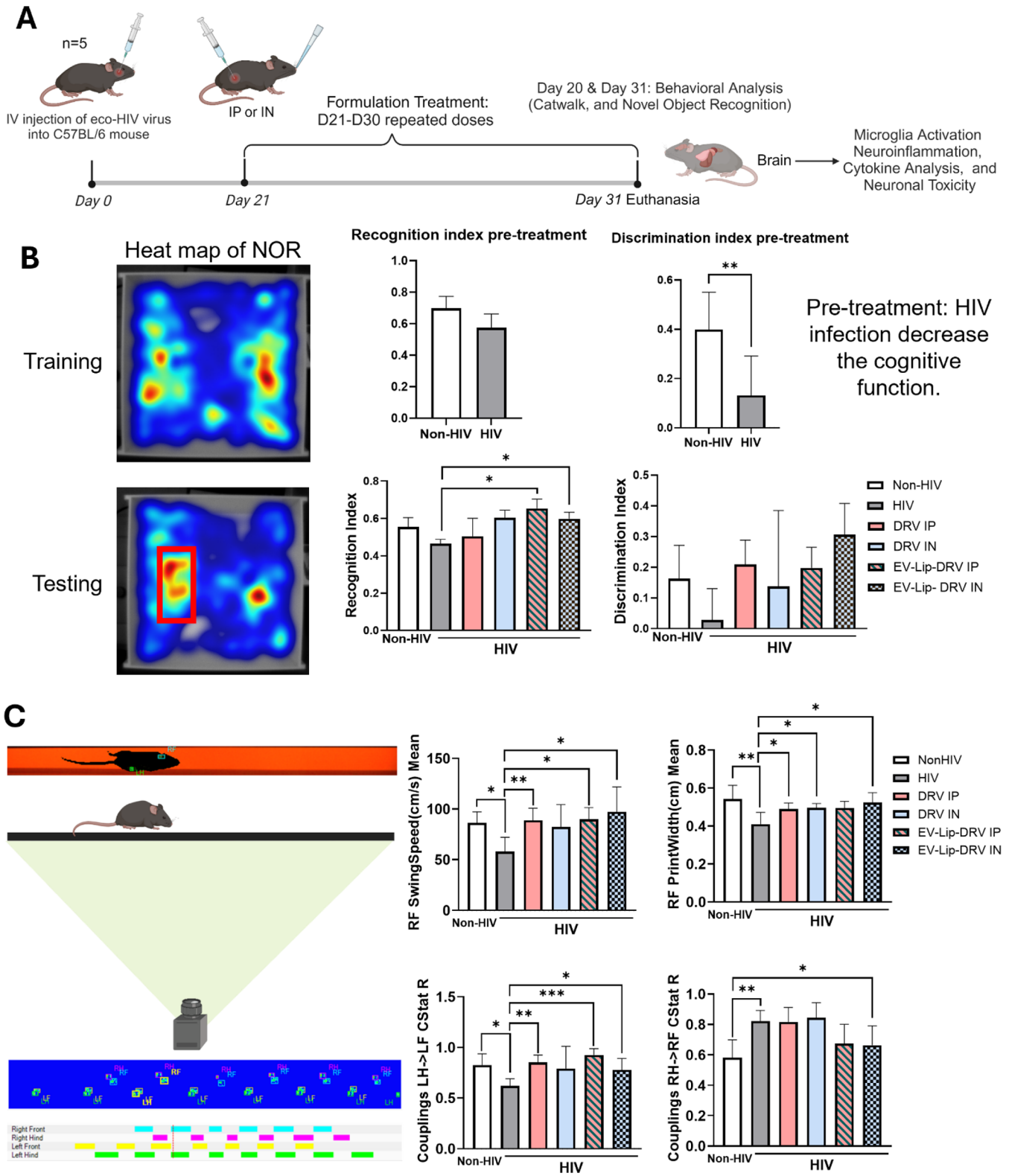

Figure 9. A. Timeline of the behavior study of mice after HIV infection and treatment with 2.5 mg/kg DRV or EV-Lip-DRV via IP or IN for 10 days. CatWalk and novel object recognition (NOR) tests were conducted to assess the motor and neurocognitive function of mice, respectively, after HIV infection. B. Heat map of the NOR test, recognition index (RI), and discrimination index (DI) were obtained before and after the DRV or EV-Lip-DRV treatment. The red square indicates the location of the new object. C. CatWalk gait analysis was recorded. Parameters with a significant difference between EcoHIV mice with and without treatment. Results are expressed as means ± SEM (n = 4−5). Statistical analysis was performed using a t test for two groups' comparisons. *: $p < 0.05$, **: $p < 0.01$, ***: $p < 0.001$.

significant changes in IL-10 or IL-1RA levels among the different treatment groups.

Overall, both EV-Lip and EV-Lip-DRV treatments modulate the cytokine and chemokine profile, significantly reducing the

https://doi.org/10.1021/acsanm.4c04637
ACS Appl. Nano Mater. 2025, 8, 6857−6876

levels of several pro-inflammatory cytokines (TNF-α, IL-1β, IL-6, IL-18), while not affecting the anti-inflammatory cytokines (IL-10 and IL-1RA). However, a decrease in the pro-inflammatory cytokine IL-8 by EV-Lip-DRV, but not by the EV-Lip formulation, suggests that the drug-encapsulated formulation may reduce the inflammatory response in U1 macrophages. Moreover, it remains to be explored further how EV-Lip alone reduces both HIV replication and pro-inflammatory cytokines but not pro-inflammatory chemokines in in vitro U1 macrophages. The lack of significant differences in pro-inflammatory cytokines among EV-Lip, DRV, and EV-Lip-DRV groups aligns with the in vitro drug exposure data presented in Figure 5. Specifically, the uptake of DRV by U1 cells was not significantly enhanced, following its encapsulation in the EV-Lip formulation. Consequently, the drug exposure of DRV in the EV-Lip-DRV group was comparable to that in the DRV group, resulting in no significant reduction in pro-inflammatory cytokines for the EV-Lip-DRV group compared to the DRV group. However, further studies are required to clarify whether EVs, liposomes, or their combination play a critical role in viral suppression and modulating the inflammatory response.

Taken together, to some extent, the EV-Lip-DRV formulation not only reduced oxidative stress but also reduced the inflammatory response in U1 macrophages. The roles of TNF-α, IL-1β, IL-6, IL-18, IL-8, IL-10, and IL-1RA are known to be associated with HIV-induced pathogenesis. The role of these cytokines and chemokines in HIV pathogenesis has been well studied in the literature and has been well discussed in our previous publication on PLGA DRV nanoparticles.[19] In brief, TNF-α, IL-1β, IL-6, IL-18, and IL-8 are key pro-inflammatory cytokines that play significant roles in the progression of HAND, which drive chronic inflammation, exacerbate neuronal damage, and contribute to cognitive decline.[54] TNF-α and IL-1β are known to mediate neuroinflammation and have been implicated in neurotoxicity, leading to neuronal apoptosis and synaptic dysfunction. IL-6 and IL-8 are involved in the recruitment of immune cells to the CNS, perpetuating the inflammatory response. IL-18, which is elevated in viral infections including HIV, also contributes to inflammation and is associated with disease severity.[55]

3.8. Permeability of DRV and EV-Lip-DRV in C57BL/6 Mice Brains. The biodistribution and pharmacokinetics of DRV and EV-Lip-DRV were evaluated in C57BL/6 wild-type mice following intraperitoneal (IP) and intranasal (IN) administration. Mice were administered 5 mg/kg of DRV via IP or 2.5 mg/kg of DRV via IN. DRV concentrations were measured in the brain, plasma, liver, and lungs after 3-h postadministration using LC-MS/MS. We selected 3 h as the terminal time point based on our previous studies which demonstrated detectable DRV concentrations in mice brains after 1 and 3 h of IN administration.[19,20] To ensure that all of the brain samples were collected at the 3 h time point, we selected 3 h as the terminal time point in this study.

As shown in Figure 8, the concentration of DRV in the brain after the indicated treatment remained unchanged via the IP administration. While there was an observed increase in brain DRV concentration in the EV-Lip-DRV group using the IN route, the variability in the data rendered these changes statistically insignificant. The brain-to-plasma ratio of DRV was calculated to assess the efficiency of brain targeting. The ratio was significantly higher for the EV-Lip-DRV group compared to the DRV group after both IP ($^{***}p < 0.001$) and IN administration ($^{*}p < 0.05$). These findings suggest that the EV-Lip-DRV formulation enhances the relative delivery and retention of DRV in the brain. Due to technical difficulties with IN administration, only half the amount of DRV was used via IN compared to IP. If similar DRV concentrations are used with both routes, the effect on DRV permeability to the brain using the IN route would be even more substantial.

To assess the off-target effect, the concentrations of DRV in the liver and lungs were also measured. No significant differences were observed between the DRV and EV-Lip-DRV groups in the liver for either administration route, though the relative DRV concentration seems to be higher in the DRV group when administered via the IP than the IN route. Similarly, in the lungs, there was a trend toward higher DRV concentration in the EV-Lip-DRV group via the IN group, though this did not reach statistical significance. Taken together, our results showed that the EV-Lip-DRV formulation using IN administration significantly increases drug distribution in the brain while reducing the off-target effects.

The results are in line with previous findings that IN improves the BBB permeability of the ART drug, which is crucial for the treatment of HIV in the CNS.[19,20,56]

Despite the advantages of IN administration, such as improved targeting and reduced systemic exposure, it is limited by the low volume that can be administered. Compared to the same IN dosing of PLGA-DRV in our earlier study, the EV-Lip-DRV showed a higher concentration of DRV and a higher brain-to-plasma ratio in the brain at 3 h. These findings suggest that the enhanced biocompatibility of the EV-Lip formulation may contribute to improved drug retention, reduced clearance, and more effective delivery to the brain.[19] PLGA nanoparticles, while effective in drug delivery, often face challenges, such as rapid clearance and potential immunogenicity. Our EV-Lip-DRV formulation can address these issues by combining the biocompatibility of EVs with the stability and drug-loading capacity of liposomes, highlighting its potential superiority over only synthetic nanoparticles.

3.9. Behavior Studies of DRV and EV-Lip-DRV in EcoHIV-Infected C57BL/6 Mice. Behavioral studies were conducted to assess the motor and neurocognitive function of EcoHIV-infected C57BL/6 mice treated with 2.5 mg/kg of DRV or EV-Lip-DRV via intraperitoneal (IP) or intranasal (IN) administration for 10 days. The timeline of the study is depicted in Figure 9A. Novel object recognition (NOR) and CatWalk gait analysis tests were performed to evaluate the treatment effects.

3.10. Cognitive Function—Novel Object Recognition (NOR) Test. Figure 9B shows the results of the NOR test. Heat maps indicate the location of the new object during the testing phase. Pretreatment assessments revealed a significant decline in cognitive function due to HIV infection, evidenced by lower recognition index (RI) and discrimination index (DI) ($^{**}p < 0.01$) values in HIV-infected mice compared to non-HIV controls.

Post-treatment assessments demonstrated improvements in cognitive function for both the DRV and EV-Lip-DRV groups using both administration routes.

Recognition index (RI): HIV-infected mice treated with EV-Lip-DRV via IP and IN administration showed significant improvement in RI compared to untreated HIV-infected controls ($^{*}p < 0.05$). However, DRV did not show a significant increase in RI using either route.

https://doi.org/10.1021/acsanm.4c04637
ACS Appl. Nano Mater. 2025, 8, 6857−6876

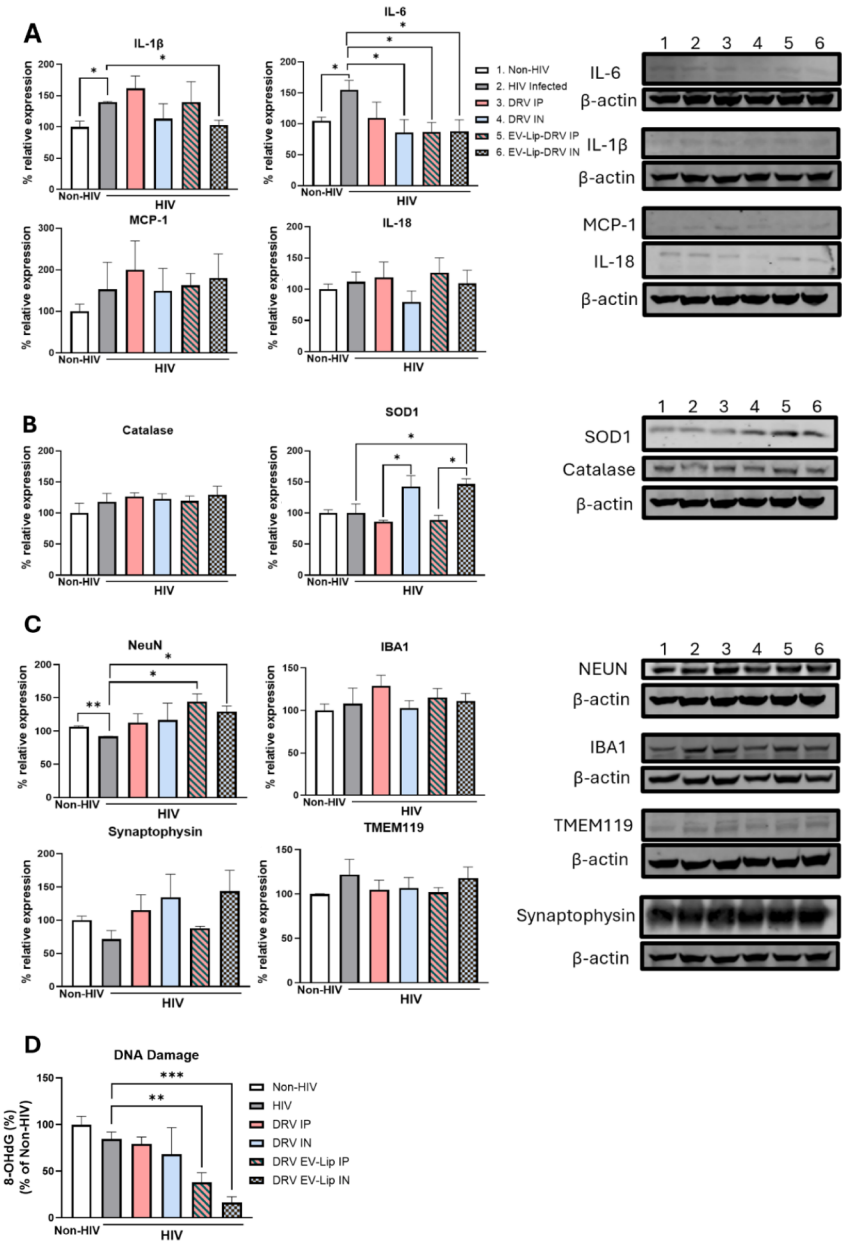

Figure 10. Western blot analysis of neural protein markers upon 10-day treatment with DRV (2.5 mg/kg) in the EcoHIV mice brain. Protein was isolated from treated mice, and expression of A. IL-1β, Il-6, MCP-1, and IL-18; B. catalase, and IBA1; C. NeuN, IBA1, synaptophysin, and TMEM119 were analyzed using Western blotting. Results are expressed as means ± SEM (n = 4). D. The extent of DNA damage in mice (n = 5) was evaluated after exposure to control or HIV infection, with and without the indicated treatments. We measured 8-OHdG, a major product of DNA oxidation, to represent DNA damage in the mice brains. The detected amount of 8-OHdG is directly proportional to the extent of DNA damage caused by the treatment. All bars are normalized against the control group. The bars represent mean ± SEM values from 5 replicates. Statistical significance was calculated using two-tailed t tests. *: $p < 0.05$, **: $p < 0.01$, ***: $p < 0.001$.

Discrimination index (DI): both DRV and EV-Lip-DRV treatments, via IP and IN routes, showed a trend in improved DI in HIV-infected mice, aligning the DI values closer to those of the non-HIV control group, but not statistically significant.

Overall, these results suggest that HIV infection impairs cognitive function, as evidenced by RI and DI, which, to some extent, is repaired by the treatment with EV-Lip-DRV, especially using IN administration.

3.11. Motor Function—CatWalk Gait Analysis. Figure 9C presents the CatWalk gait analysis results. Several parameters showed significant differences between uninfected and EcoHIV-infected and between the control and treated groups in EcoHIV-infected mice. However, here, we present only four parameters.

RF swing speed: HIV-infected mice showed a reduced right front (RF) swing speed compared to the non-HIV control. Treatment with DRV and EV-Lip-DRV via both IP and IN routes significantly improved the RF swing speed, with notable increases. However, there was no difference between DRV alone and EV-Lip-DRV or between the two routes of administration.

RF print width: the HIV-infected group exhibited a narrower RF print width compared to non-HIV control. Both DRV (IP and IN) and EV-Lip-DRV (IN) treatments led to a significant

https://doi.org/10.1021/acsanm.4c04637
ACS Appl. Nano Mater. 2025, 8, 6857−6876

increase in RF print width, indicating improved motor function.

HIV-infected mice displayed altered couplings between left hind-left front (LH-LF) and right hind-right front (RH-RF) limbs, with significant deviations from the non-HIV control group. Treatments with DRV (IP) and EV-Lip-DRV (IP and IN) normalized left hind-left front (LH-LF) couplings, bringing them closer to control values with significant improvement observed, which was similar to the observations in RF swing speed. Only EV-Lip-DRV via IN significantly improved the coupling of right hind-right front (RH-RF) limbs.

These results suggest that HIV infection impairs motor function, as evidenced by changes in the RF swing speed, RF print width, and limb couplings. Treatment with DRV and EV-Lip-DRV effectively ameliorates these motor deficits, demonstrating the potential of both DRV and the formulation to restore motor function in HIV-infected mice, especially via the IN route.

With the progression of HIV, patients have a range of cognitive, motor, and behavioral symptoms, which are hallmarks of HAND. The NOR test and CatWalk gait analysis were employed to evaluate cognitive and motor functions in HIV-infected mice, respectively. The findings from the NOR test suggest that HIV-infected mice have reduced cognitive function, which to some extent is recovered by the treatment group, especially with EV-Lip-DRV using the IN route. The CatWalk gait analysis reveals impairments in motor function by HIV infection, which to some extent is recovered by the EV-Lip-DRV treatment. Although CatWalk is not a typical test for HAND, it is used to measure movement disorders in Parkinson's disease (PD) and Huntington's disease (HD).[57] Since CatWalk measures motor, emotional, and cognitive deficits in HD, which are also characteristics of HAND, we use the test to measure motor and cognitive functions in HIV. Thus, in addition to NOR, the CatWalk test can also be used to study behavior deficits in HIV mice. Taken together, our findings suggest that a daily dose of EV-Lip-DRV via the IN route may offer a potentially novel therapeutic approach for managing neurocognitive and motor dysfunctions associated with HIV.

We acknowledge that there is no perfect animal model to study HAND. The rodent models to study HAND were well-discussed earlier.[58] We selected the EcoHIV mouse model mainly because it is a well-established HIV mouse model featuring behavioral deficits and neuropathological changes upon infection.[59] Various behavior studies indicate cognitive (NOR, Morris water maze, Barnes maze, contextual and cued fear conditioning, etc.), and motor (rotarod test, grip strength test, ladder rung walking test, etc.)[58] functions that may be used to study HAND in HIV mice. Nose-to-brain delivery has been explored for HIV treatment; however, most of those studies focused on the improvement of brain drug concentration and its effect on HIV biomarkers. However, a few of them evaluated the behavior of mice. We found a study showing that IN administration of insulin for 9 days reduces HIV DNA in the brain for a short term leading to improved performance of HIV mice in the radial arm water maze study.[60] According to our knowledge, our study is the first one to show improvement in cognition and motor functions in HIV mice by EV-Lip formulation using the IN route. However, future efforts are needed to optimize the encapsulation efficiency, understand cellular uptake mechanisms, and tailor formulations for different ART drugs.

3.12. Effect of EV-Lip-DRV on Neuroinflammation, Neuronal Damage, and Oxidative Stress in EcoHIV Mice. We analyzed the protein expression of inflammatory cytokines and chemokines, oxidative stress markers, and neuronal markers in mouse brains with and without EcoHIV infection.

Figure 10A presents the Western blot results for representative inflammatory cytokines IL-1β, IL-6, IL-18, and the chemokine MCP-1 in the brains of HIV-infected mice. As expected, HIV infection significantly elevated IL-1β and IL-6 levels. Treatment with EV-Lip-DRV via IN administration significantly reduced IL-1β and IL-6 levels ($^*p < 0.05$). Although DRV via IP administration also reduced IL-1β levels, the change was not statistically significant. DRV via the IN route and EV-Lip-DRV via the IP route also significantly reduced IL-6 levels ($^*p < 0.05$). No significant changes in MCP-1 and IL-18 levels were observed in the HIV-infected group compared to the uninfected group, and among the different treatment groups compared to the nontreated group in EcoHIV.

Figure 10B shows the Western blot results for oxidative stress markers, catalase, and SOD1. HIV infection increased SOD1 levels, indicating elevated oxidative stress. Treatment with DRV and EV-Lip-DRV via IN administration significantly reduced SOD1 levels ($^*p < 0.05$). However, catalase levels remained similar across all groups, suggesting no significant changes in this oxidative stress marker.

Figure 10C displays the Western blot results for neuronal markers (NeuN, synaptophysin) and microglia markers (IBA1 and TMEM119). NeuN is a nuclear protein expressed in most neuronal cells indicating differentiation of neurons. IBA1 and TMEM119 are microglia markers indicating microglia activation and surface protein, respectively. Synaptophysin serves as a marker for synapses, which is used to study synaptogenesis, synaptic density, and changes in synaptic connections in various neurological conditions.[61] HIV infection significantly reduced NeuN levels compared to non-HIV control ($^{**}p < 0.01$). Treatment with EV-Lip-DRV via both IP and IN significantly increased NeuN levels ($^*p < 0.05$). No significant changes were observed in IBA1 and TMEM119 levels among the different groups. Although synaptophysin levels were decreased in HIV-infected mice and showed an increase in the treatment groups, these changes were not statistically significant.

The extent of DNA damage was evaluated by measuring 8-OHdG levels, which are markers of DNA oxidation, in the brains of mice. As shown in Figure 10D, treatment with EV-Lip-DRV, particularly via IP and IN administration, significantly reduced 8-OHdG levels compared to untreated HIV-infected mice ($^{**}p < 0.01$, $^{***}p < 0.001$), indicating a reduction in DNA damage. However, no significant change was observed in DRV treatment regardless of the routes.

As noted before, the EV-Lip-DRV formulation modulates the cytokine and chemokine profile, decreasing pro-inflammatory markers (TNF-α, IL-1β, IL-6, IL-18, IL-8) without affecting anti-inflammatory cytokines (IL-10, IL-1RA) in U1 macrophages. The reduction of TNF-α, IL-1β, IL-6, and IL-18 in EV-Lip treatment in vitro may be caused by the activation of NF-kB pathway as the study showed MSC-derived EV can mitigate the overexpression of inflammatory cytokines in the mice liver cell line.[62] We observed decreased levels of IL-6 in

https://doi.org/10.1021/acsanm.4c04637
ACS Appl. Nano Mater. 2025, 8, 6857−6876

DRV IN and EV-Lip-DRV of both routes (IP and IN) in HIV mice brains. The reduction of IL-6 in the brains of HIV-infected mice treated with DRV IN and EV-Lip-DRV via IP and IN administration in our study is consistent with the findings of Rodriguez et al., who observed similar results when dosing siBeclin1-PEI-Man Nanoplex via IN in EcoHIV mice.[63] Their study also showed ART treatment reduced MCP-1 expression in EcoHIV mice brain,[64] which is similar to our finding. The inflammatory response in the brain has been strongly correlated with cognitive impairment in EcoHIV mice.[64] Modulating the levels of inflammatory cytokines and chemokines is one of the mechanisms by which the EV-Lip-DRV formulation may mitigate HAND.

In the context of HIV infection, chronic inflammation and viral proteins contribute to increased ROS production, leading to neuronal damage and apoptosis. This oxidative damage, combined with neuroinflammation, exacerbates the neurocognitive decline observed in HAND patients.[65] In our study, EV-Lip-DRV treatment increased SOD1 expression, suggesting that EV-Lip-DRV can protect the cells from oxidative damage in EcoHIV mice brain. This notion is further strengthened by our observation that EV-Lip-DRV reduces the level of oxidative DNA damage in EcoHIV mice. In addition, our in vitro data with U1 macrophages in which EV-Lip-DRV treatment reduces the ROS level is consistent with an in vivo study with EcoHIV mice where the treatment reduces oxidative stress/DNA damage. Together, these findings suggest a decrease in the level of oxidative stress upon treatment with EV-Lip-DRV in EcoHIV mice.

On the other hand, Ogedengbe et al. have shown that ART treatment reduces SOD1 and catalase in healthy Wistar rats.[66] Moreover, our previous study on the coadministration of curcumin and elvitegravir in healthy Balb/c mice has also shown a reduction of SOD1 in mice brain.[49] This discrepancy may occur because 1) our current study was performed in EcoHIV mice vs wild-type mice in other studies and 2) our current study uses EV-Lip-DRV formulation, while another study was performed with ART drug and/or curcumin treatment. In addition, the differences in the treatment times in these studies may also account for the differences.

HIV is known to reduce the levels of NeuN. For example, Honeycutt et al. observed a decrease in the number of $NeuN^+$ neurons in the HIV-infected humanized mouse model.[67] Consistent with the literature, our study also shows a decrease in NeuN in EcoHIV. More importantly, increased levels of NenN upon EV-Lip-DRV treatment suggest recovery of neuronal differentiation from HIV infection.

A study by Honeycutt et al. shows an increase in IBA1 and subsequent microglial activation in HIV-infected mice upon inflammation induced by HIV in the brain.[67] However, our current finding is not consistent with the literature, perhaps because we used the EcoHIV mice model as opposed to the use of the humanized bone marrow/liver/thymus (BLT) mouse model in the study performed by Honeycutt et al.

Gene expression of TMEM119 is significantly down-regulated after homeostasis is disturbed in the brain.[68] The microglial homeostasis upon EcoHIV infection and treatment with EV-Lip-DRV in our study appears to be maintained, indicated by no change in the levels of TMEM119 among all groups. Akay et al. showed a reduction in synaptophysin levels in the hippocampi of the SIV macaques subcutaneously treated with ART drugs for 12 days compared to the uninfected and SIV(+)/placebo group.[16] They suggest that the SIV infection and drug treatment together induce neuronal damage. In contrast, our study did not significantly alter the level of synaptophysin either by HIV infection or by drug treatment. HIV infection appears to decrease its level, while EV-Lip-DRV treatment appears to rescue the decrease caused by HIV infection, suggesting that EV-Lip-DRV may help recover neuronal damage induced by HIV.

3.13. Limitations of Current Study and Future Plans.

The classification of EVs as biological products during the approval process presents significant regulatory challenges when they are fused with liposomes. This fusion introduces complexities that must be addressed from a regulatory perspective. Future perspectives include refining manufacturing techniques to ensure consistency and scalability as well as developing standardized regulatory frameworks to streamline clinical translation.

It has been reported that ART-loaded nanolipid carriers induce certain morphological changes in mice brains after IN administration, though their effect on functional changes remains unknown.[69] In our study, we have seen improvement in HAND after treatment with EV-Lip-DRV in EcoHIV mice. However, we have not yet assessed the impact of EV-Lip-DRV on brain morphology and function in healthy mice, which will be addressed in future research. A long-term safety assessment of EV-Lip and EV-Lip-ART using biomarkers in peripheral organs such as the liver, lungs, and spleen is necessary.

The nasal anatomy of mice and humans differs significantly, affecting the intranasal drug delivery. Mice have a larger nasal cavity relative to their size, with a higher surface area-to-volume ratio and more complex nasal turbinates,[70] leading to differences in drug deposition, absorption, and mucociliary clearance. Further studies are needed to optimize the method of intranasal delivery of EV-Lip formulations to bridge preclinical and clinical studies.

Although the development of EV-liposome formulations is still in its infancy and there are regulatory concerns as well as challenges in the manufacturing processes, this approach represents a promising drug delivery platform for diagnostics and targeted therapy. As our understanding of the functions and roles of EVs in the body expands, the potential applications of EV-liposome systems are expected to grow significantly. Future perspectives include the refinement of manufacturing techniques to ensure consistency and scalability along with the development of standardized regulatory frameworks. Furthermore, the exploration of EV-Lip formulations for personalized medicine is anticipated to yield significant advancements.[41] Additionally, advancements in nanotechnology could enhance the stability, targeting specificity, and therapeutic efficacy of these hybrid systems. Such improvements will pave the way for more effective treatments for a variety of neurological disorders beyond HIV neuropathogenesis. Overall, the integration of EVs into liposome-based drug delivery systems holds great promise for revolutionizing the landscape of targeted brain therapies.

4. CONCLUSIONS

This study provides compelling evidence that the EV-Lip-ART drug delivery system can ameliorate symptoms associated with characteristics of HIV neuropathogenesis, including HAND in EcoHIV mice. By leveraging the benefits of EVs and liposomes, we achieved significant improvements in drug delivery across the BBB, stability, and therapeutic outcomes. The EV-Lip-DRV formulation demonstrated reasonable stability, excellent

https://doi.org/10.1021/acsanm.4c04637
ACS Appl. Nano Mater. 2025, 8, 6857−6876

hemocompatibility, and the ability to maintain drug release profiles. The formulation also shows the potential to reduce oxidative stress, inflammation, and neuronal damage, especially caused by HIV infection. Our findings underscore the potential of EV-Lip nanoparticles for addressing the challenges of HIV neuropathogenesis and potentially other neurological disorders.

AUTHOR INFORMATION

Corresponding Author

Santosh Kumar − *Department of Pharmaceutical Sciences, University of Tennessee Health Science Center, Memphis, Tennessee 38163, United States;* orcid.org/0000-0001-7846-5674; Email: ksantosh@uthsc.edu

Authors

Lina Zhou − *Department of Pharmaceutical Sciences, University of Tennessee Health Science Center, Memphis, Tennessee 38163, United States*

Sandip Godse − *Department of Pharmaceutical Sciences, University of Tennessee Health Science Center, Memphis, Tennessee 38163, United States*

Namita Sinha − *Department of Pharmaceutical Sciences, University of Tennessee Health Science Center, Memphis, Tennessee 38163, United States*

Dejian Ma − *Department of Pharmaceutical Sciences, University of Tennessee Health Science Center, Memphis, Tennessee 38163, United States*

Golnoush Mirzahosseini − *Department of Pharmaceutical Sciences, University of Tennessee Health Science Center, Memphis, Tennessee 38163, United States; Department of Anatomy and Neurobiology, College of Medicine, The University of Tennessee Health Science Center, Memphis, Tennessee 38163, United States*

Mohd Salman − *Department of Anatomy and Neurobiology, College of Medicine, The University of Tennessee Health Science Center, Memphis, Tennessee 38163, United States*

Paul Pulliam − *Plough Center for Sterile Drug Delivery Solutions, University of Tennessee Health Science Center, Memphis, Tennessee 38163, United States*

Chalet Tan − *Department of Pharmaceutical Sciences, University of Tennessee Health Science Center, Memphis, Tennessee 38163, United States*

Udai P. Singh − *Department of Pharmaceutical Sciences, University of Tennessee Health Science Center, Memphis, Tennessee 38163, United States*

Tauheed Ishrat − *Department of Anatomy and Neurobiology, College of Medicine, The University of Tennessee Health Science Center, Memphis, Tennessee 38163, United States*

Harry Kochat − *Department of Pharmaceutical Sciences, University of Tennessee Health Science Center, Memphis, Tennessee 38163, United States; Plough Center for Sterile Drug Delivery Solutions, University of Tennessee Health Science Center, Memphis, Tennessee 38163, United States*

Complete contact information is available at: https://pubs.acs.org/10.1021/acsanm.4c04637

Author Contributions

Conceptualization: L.Z. and S.K.; methodology: L.Z., D.M., M.S., P.P., C.T., U.S., T.I., and H.K.; investigation: S.G., N.S., D.M., G.M., and P.P.; validation: L.Z., S.G., and N.S.; formal analysis: L.Z. and S.K.; resources: S.K., U.S., T.I., and H.K.; writing—original draft: L.Z. and S.K.; writing—review and editing: All authors; visualization: L.Z.; supervision: S.K.; project administration: S.K. The manuscript was written through the contributions of all authors. All authors have approved the final version of the manuscript.

Funding

This research was funded by the National Institutes of Health grants AG081140 and MH125670, and funding from the UTHSC Plow Center to Santosh Kumar as well as a grant for an independent research project from the University of Tennessee Health Science Center to Lina Zhou.

Notes

The authors declare no competing financial interest.

ACKNOWLEDGMENTS

We acknowledge the Imaging Center Microscopy Service at UTHSC for the use of TEM (JEOL-2000EX, Tokyo, Japan) and the Analytical Facility for the UTHSC College of Pharmacy for the use of LC-MS/MS. The SCIEX 5500 LC-MS is funded by NIH S10 grant 1S10OD016226-01A1. We also appreciate the technical support from Dr. Giorgia Pastorin's group during the initial setup of the method for EV-Lip hybrid production. Figures cover graphic, 1, 2A, 3A,B, and 9A and the timeline in Figure 8 were created using Biorender.

REFERENCES

(1) Wang, Y.; Liu, M.; Lu, Q.; Farrell, M.; Lappin, J. M.; Shi, J.; Lu, L.; Bao, Y. Global prevalence and burden of HIV-associated neurocognitive disorder. *Neurology* **2020**, *95* (19), No. e2610−e2621.

(2) Valcour, V.; Chalermchai, T.; Sailasuta, N.; Marovich, M.; Lerdlum, S.; Suttichom, D.; Suwanwela, N. C.; Jagodzinski, L.; Michael, N.; Spudich, S.; et al. Central Nervous System Viral Invasion and Inflammation During Acute HIV Infection. *J. Infect. Dis.* **2012**, *206* (2), 275−282.

(3) Borrajo, A.; Spuch, C.; Penedo, M. A.; Olivares, J. M.; Agís-Balboa, R. C. Important role of microglia in HIV-1 associated neurocognitive disorders and the molecular pathways implicated in its pathogenesis. *Ann. Med.* **2021**, *53* (1), 43−69.

(4) Al-Harti, L.; Joseph, J.; Nath, A. Astrocytes as an HIV CNS reservoir: Highlights and reflections of an NIMH-sponsored symposium. *J. Neurovirol.* **2018**, *24* (6), 665−669.

(5) Luissint, A.-C.; Artus, C.; Glacial, F.; Ganeshamoorthy, K.; Couraud, P.-O. Tight junctions at the blood brain barrier: Physiological architecture and disease-associated dysregulation. *Fluids Barriers CNS* **2012**, *9* (1), 23.

(6) de Jong, O. G.; Kooijmans, S. A. A.; Murphy, D. E.; Jiang, L.; Evers, M. J. W.; Sluijter, J. P. G.; Vader, P.; Schiffelers, R. M. Drug Delivery with Extracellular Vesicles: From Imagination to Innovation. *Acc. Chem. Res.* **2019**, *52* (7), 1761−1770.

(7) Zhou, L.; Kodidela, S.; Godse, S.; Thomas-Gooch, S.; Kumar, A.; Raji, B.; Zhi, K.; Kochat, H.; Kumar, S. Targeted Drug Delivery to the Central Nervous System Using Extracellular Vesicles. *Pharmaceuticals* **2022**, *15* (3), 358.

(8) Rosso, G.; Cauda, V. Biomimicking Extracellular Vesicles with Fully Artificial Ones: A Rational Design of EV-BIOMIMETICS toward Effective Theranostic Tools in Nanomedicine. *ACS Biomater. Sci. Eng.* **2023**, *9* (11), 5924−5932.

(9) Swenson, C. E.; Perkins, W. R.; Roberts, P.; Janoff, A. S. Liposome technology and the development of Myocet (liposomal doxorubicin citrate). *Breast* **2001**, *10*, 1−7.

(10) Hu, Y.; Li, X.; Zhang, Q.; Gu, Z.; Luo, Y.; Guo, J.; Wang, X.; Jing, Y.; Chen, X.; Su, J. Exosome-guided bone targeted delivery of Antagomir-188 as an anabolic therapy for bone loss. *Bioact. Mater.* **2021**, *6* (9), 2905−2913.

(11) Lv, Q.; Cheng, L.; Lu, Y.; Zhang, X.; Wang, Y.; Deng, J.; Zhou, J.; Liu, B.; Liu, J. Thermosensitive Exosome-Liposome Hybrid

Nanoparticle-Mediated Chemoimmunotherapy for Improved Treatment of Metastatic Peritoneal Cancer. *Adv. Sci.* **2020**, *7* (18), 2000515.
(12) Goh, W. J.; Zou, S.; Czarny, B.; Pastorin, G. nCVTs: A hybrid smart tumour targeting platform. *Nanoscale* **2018**, *10* (15), 6812−6819.
(13) Staufer, O.; Dietrich, F.; Rimal, R.; Schröter, M.; Fabritz, S.; Boehm, H.; Singh, S.; Möller, M.; Platzman, I.; Spatz, J. P. Bottom-up assembly of biomedical relevant fully synthetic extracellular vesicles. *Sci. Adv.* **2021**, *7* (36), No. eabg6666.
(14) Schrijvers, R.; Debyser, Z. Combinational therapies for HIV: A focus on EVG/COBI/FTC/TDF. *Expert Opin. Pharmacother.* **2012**, *13* (13), 1969−1983.
(15) Kakuda, T. N.; Opsomer, M.; Timmers, M.; Iterbeke, K.; Van De Casteele, T.; Hillewaert, V.; Petrovic, R.; Hoetelmans, R. M. Pharmacokinetics of darunavir in fixed-dose combination with cobicistat compared with coadministration of darunavir and ritonavir as single agents in healthy volunteers. *J. Clin. Pharmacol.* **2014**, *54* (8), 949−957.
(16) Akay, C.; Cooper, M.; Odeleye, A.; Jensen, B. K.; White, M. G.; Vassoler, F.; Gannon, P. J.; Mankowski, J.; Dorsey, J. L.; Buch, A. M.; Cross, S. A.; Cook, D. R.; Peña, M.-M.; Andersen, E. S.; Christofidou-Solomidou, M.; Lindl, K. A.; Zink, M. C.; Clements, J.; Pierce, R. C.; Kolson, D. L.; Jordan-Sciutto, K. L. Antiretroviral drugs induce oxidative stress and neuronal damage in the central nervous system. *J. NeuroVirol.* **2014**, *20* (1), 39−53.
(17) Curran, A.; Gutierrez, M.; Deig, E.; Mateo, G.; Lopez, R. M.; Imaz, A.; Crespo, M.; Ocana, I.; Domingo, P.; Ribera, E. Efficacy, safety and pharmacokinetics of 900/100 mg of darunavir/ritonavir once daily in treatment-experienced patients. *J. Antimicrob. Chemother.* **2010**, *65* (10), 2195−2203.
(18) Ferrara, M.; Bumpus, N. N.; Ma, Q.; Ellis, R. J.; Soontornniyomkij, V.; Fields, J. A.; Bharti, A.; Achim, C. L.; Moore, D. J.; Letendre, S. L. Antiretroviral drug concentrations in brain tissue of adult decedents. *Aids* **2020**, *34* (13), 1907−1914.
(19) Zhou, L.; Godse, S.; Sinha, N.; Kodidela, S.; Singh, U.; Kumar, S. Darunavir Nanoformulation Suppresses HIV Pathogenesis in Macrophages and Improves Drug Delivery to the Brain in Mice. *Pharmaceutics* **2024**, *16* (4), 555.
(20) Kumar, A.; Zhou, L.; Godse, S.; Sinha, N.; Ma, D.; Parmar, K.; Kumar, S. Intranasal delivery of darunavir improves brain drug concentrations in mice for effective HIV treatment. *Biochem. Biophys. Rep.* **2023**, *33*, 101408.
(21) Yallapu, M. M.; Chauhan, N.; Othman, S. F.; Khalilzad-Sharghi, V.; Ebeling, M. C.; Khan, S.; Jaggi, M.; Chauhan, S. C. Implications of protein corona on physico-chemical and biological properties of magnetic nanoparticles. *Biomaterials* **2015**, *46*, 1−12.
(22) Alfar, H. R.; Pariser, D. N.; Chanzu, H.; Joshi, S.; Coenen, D. M.; Lykins, J.; Prakhya, K. S.; Potash, M. J.; Chao, W.; Kelschenbach, J.; Volsky, D. J.; Metcalf-Pate, K.; Whiteheart, S. W. Protocol for optimizing production and quality control of infective EcoHIV virions. *STAR Protoc.* **2023**, *4* (3), 102368.
(23) Ahmed, H. A.; Ismael, S.; Mirzahosseini, G.; Ishrat, T. Verapamil Prevents Development of Cognitive Impairment in an Aged Mouse Model of Sporadic Alzheimer's Disease. *Mol. Neurobiol.* **2021**, *58* (7), 3374−3387.
(24) Salman, M.; Ismael, S.; Ishrat, T. A modified murine photothrombotic stroke model: A minimally invasive and reproducible cortical and sub-cortical infarct volume and long-term deficits. *Exp. Brain Res.* **2023**, *241* (10), 2487−2497.
(25) Herrmann, I. K.; Wood, M. J. A.; Fuhrmann, G. Extracellular vesicles as a next-generation drug delivery platform. *Nat. Nanotechnol.* **2021**, *16* (7), 748−759.
(26) Kumar, A.; Zhou, L.; Zhi, K.; Raji, B.; Pernell, S.; Tadrous, E.; Kodidela, S.; Nookala, A.; Kochat, H.; Kumar, S. Challenges in Biomaterial-Based Drug Delivery Approach for the Treatment of Neurodegenerative Diseases: Opportunities for Extracellular Vesicles. *Int. J. Mol. Sci.* **2021**, *22* (1), 138.
(27) Juhairiyah, F.; de Lange, E. C. M. Understanding Drug Delivery to the Brain Using Liposome-Based Strategies: Studies that Provide Mechanistic Insights Are Essential. *Aaps J.* **2021**, *23* (6), 114.
(28) Mitchell, M. J.; Billingsley, M. M.; Haley, R. M.; Wechsler, M. E.; Peppas, N. A.; Langer, R. Engineering precision nanoparticles for drug delivery. *Nat. Rev. Drug Discovery* **2021**, *20* (2), 101−124.
(29) Ducrot, C.; Loiseau, S.; Wong, C.; Madec, E.; Volatron, J.; Piffoux, M. Hybrid extracellular vesicles for drug delivery. *Cancer Lett.* **2023**, *558*, 216107.
(30) Wang, R.; Wang, X.; Zhao, H.; Li, N.; Li, J.; Zhang, H.; Di, L. Targeted delivery of hybrid nanovesicles for enhanced brain penetration to achieve synergistic therapy of glioma. *J. Controlled Release* **2024**, *365*, 331−347.
(31) Geng, T.; Tang, M.; Yee Paek, S.; Leung, E.; Chamley, L. W.; Wu, Z. A simple approach to re-engineering small extracellular vesicles to circumvent endosome entrapment. *Int. J. Pharm.* **2022**, *626*, 122153.
(32) Shafique, M.; Ur Rehman, M.; Kamal, Z.; Alzhrani, R. M.; Alshehri, S.; Alamri, A. H.; Bakkari, M. A.; Sabei, F. Y.; Safhi, A. Y.; Mohammed, A. M.; Hamd, M. A. E.; Almawash, S. Formulation development of lipid polymer hybrid nanoparticles of doxorubicin and its in-vitro, in-vivo and computational evaluation. *Front. Pharmacol.* **2023**, *14*, 1025013.
(33) Paschoal Barbosa, L. M.; Gomes, E. R.; Barros, A. L. B. D.; Cassali, G. D.; Carvalho, A. T. D.; Silva, J. D. O.; Pádua, A. L.; Oliveira, M. C. Hybrid Nanosystem Formed by DOX-Loaded Liposomes and Extracellular Vesicles from MDA-MB-231 Is Effective against Breast Cancer Cells with Different Molecular Profiles. *Pharmaceutics* **2024**, *16* (6), 739.
(34) Maroto, R.; Zhao, Y.; Jamaluddin, M.; Popov, V. L.; Wang, H.; Kalubowilage, M.; Zhang, Y.; Luisi, J.; Sun, H.; Culbertson, C. T.; Bossmann, S. H.; Motamedi, M.; Brasier, A. R. Effects of storage temperature on airway exosome integrity for diagnostic and functional analyses. *J. Extracell. Vesicles* **2017**, *6* (1), 1359478.
(35) Sun, L.; Fan, M.; Huang, D.; Li, B.; Xu, R.; Gao, F.; Chen, Y. Clodronate-loaded liposomal and fibroblast-derived exosomal hybrid system for enhanced drug delivery to pulmonary fibrosis. *Biomaterials* **2021**, *271*, 120761.
(36) Rayamajhi, S.; Nguyen, T. D. T.; Marasini, R.; Aryal, S. Macrophage-derived exosome-mimetic hybrid vesicles for tumor targeted drug delivery. *Acta Biomater.* **2019**, *94*, 482−494.
(37) Cheng, Y.; Zeng, Q.; Han, Q.; Xia, W. Effect of pH, temperature and freezing-thawing on quantity changes and cellular uptake of exosomes. *Protein Cell* **2019**, *10* (4), 295−299.
(38) Lőrincz, Á. M.; Timár, C. I.; Marosvári, K. A.; Veres, D. S.; Otrokocsi, L.; Kittel, Á.; Ligeti, E. Effect of storage on physical and functional properties of extracellular vesicles derived from neutrophilic granulocytes. *J. Extracell. Vesicles* **2014**, *3*, 25465.
(39) *Package Insert - SPIKEVAX*. https://www.fda.gov/vaccines-blood-biologics/spikevax.
(40) *Package Insert - COMIRNATY*. https://www.fda.gov/vaccines-blood-biologics/comirnaty.
(41) Piffoux, M.; Silva, A. K. A.; Wilhelm, C.; Gazeau, F.; Tareste, D. Modification of Extracellular Vesicles by Fusion with Liposomes for the Design of Personalized Biogenic Drug Delivery Systems. *ACS Nano* **2018**, *12* (7), 6830−6842.
(42) Wang, X.; Li, D.; Li, G.; Chen, J.; Yang, Y.; Bian, L.; Zhou, J.; Wu, Y.; Chen, Y. Enhanced Therapeutic Potential of Hybrid Exosomes Loaded with Paclitaxel for Cancer Therapy. *Int. J. Mol. Sci.* **2024**, *25* (7), 3645.
(43) Gomes, E. R.; Carvalho, A. T.; Barbosa, T. C.; Ferreira, L. L.; Calado, H. D. R.; Sabino, A. P.; Oliveira, M. C. Fusion of Tumor-Derived Exosomes with Long-Circulating and pH-Sensitive Liposomes Loaded with Doxorubicin for the Treatment of Breast Cancer. *AAPS PharmScitech* **2022**, *23* (7), 255.
(44) Kim, S. Y.; Guk, D.; Jeong, Y.; Kim, E.; Kim, H.; Kim, S. T. Engineered Hybrid Vesicles and Cellular Internalization in Mammary Cancer Cells. *Pharmaceutics* **2024**, *16* (4), 440.

https://doi.org/10.1021/acsanm.4c04637
ACS Appl. Nano Mater. 2025, 8, 6857−6876

(45) Evers, M. J. W.; van de Wakker, S. I.; de Groot, E. M.; de Jong, O. G.; Gitz-François, J. J. J.; Seinen, C. S.; Sluijter, J. P. G.; Schiffelers, R. M.; Vader, P. Functional siRNA Delivery by Extracellular Vesicle−Liposome Hybrid Nanoparticles. *Adv. Healthcare Mater.* **2022**, *11* (5), 2101202.
(46) Madison, M. N.; Roller, R. J.; Okeoma, C. M. Human semen contains exosomes with potent anti-HIV-1 activity. *Retrovirology* **2014**, *11* (1), 102.
(47) Tumne, A.; Prasad, V. S.; Chen, Y.; Stolz, D. B.; Saha, K.; Ratner, D. M.; Ding, M.; Watkins, S. C.; Gupta, P. Noncytotoxic Suppression of Human Immunodeficiency Virus Type 1 Transcription by Exosomes Secreted from $CD8^+$ T Cells. *J. Virol.* **2009**, *83* (9), 4354−4364.
(48) Konopka, K.; Davis, B. R.; Larsen, C. E.; Düzgüneş, N. Anionic Liposomes Inhibit Human Immunodeficiency Virus Type 1 (HIV-1) Infectivity in CD4+ A3.01 and H9 Cells. *Antiviral Chem. Chemother.* **1993**, *4* (3), 179−187.
(49) Godse, S.; Zhou, L.; Sinha, N.; Kodidela, S.; Kumar, A.; Singh, U. P.; Kumar, S. Curcumin enhances elvitegravir concentration and alleviates oxidative stress and inflammatory response. *Sci. Rep.* **2023**, *13* (1), 19864.
(50) Ivanov, A. V.; Valuev-Elliston, V. T.; Ivanova, O. N.; Kochetkov, S. N.; Starodubova, E. S.; Bartosch, B.; Isaguliants, M. G. Oxidative Stress during HIV Infection: Mechanisms and Consequences. *Oxid. Med. Cell. Longev.* **2016**, *2016* (1), 8910396.
(51) Shi, B.; De Girolami, U.; He, J.; Wang, S.; Lorenzo, A.; Busciglio, J.; Gabuzda, D. Apoptosis induced by HIV-1 infection of the central nervous system. *J. Clin. Invest.* **1996**, *98* (9), 1979−1990.
(52) Chettimada, S.; Lorenz, D. R.; Misra, V.; Dillon, S. T.; Reeves, R. K.; Manickam, C.; Morgello, S.; Kirk, G. D.; Mehta, S. H.; Gabuzda, D. Exosome markers associated with immune activation and oxidative stress in HIV patients on antiretroviral therapy. *Sci. Rep.* **2018**, *8* (1), 7227.
(53) Welch, J. L.; Kaddour, H.; Winchester, L.; Fletcher, C. V.; Stapleton, J. T.; Okeoma, C. M. Semen Extracellular Vesicles From HIV-1-Infected Individuals Inhibit HIV-1 Replication In Vitro, and Extracellular Vesicles Carry Antiretroviral Drugs In Vivo. *J. Acquir. Immune Defic. Syndr.* **2020**, *83* (1), 90−98.
(54) Tatro, E. T.; Soontornniyomkij, B.; Letendre, S. L.; Achim, C. L. Cytokine secretion from brain macrophages infected with human immunodeficiency virus in vitro and treated with raltegravir. *BMC Infect. Dis.* **2014**, *14* (1), 386.
(55) Feria, M. G.; Taborda, N. A.; Hernandez, J. C.; Rugeles, M. T. HIV replication is associated to inflammasomes activation, IL-1β, IL-18 and caspase-1 expression in GALT and peripheral blood. *PLoS One* **2018**, *13* (4), No. e0192845.
(56) Mehrotra, S.; Salwa; Bg, P. K.; Bhaskaran, N. A.; Srinivas Reddy, J.; Kumar, L. Nose-to-Brain delivery of antiretroviral drug loaded lipidic nanocarriers to purge HIV reservoirs in CNS: A safer approach. *J. Drug Delivery Sci. Technol.* **2023**, *87*, 104833.
(57) Vandeputte, C.; Taymans, J. M.; Casteels, C.; Coun, F.; Ni, Y.; Van Laere, K.; Baekelandt, V. Automated quantitative gait analysis in animal models of movement disorders. *BMC Neurosci.* **2010**, *11*, 92.
(58) Gorantla, S.; Poluektova, L.; Gendelman, H. E. Rodent models for HIV-associated neurocognitive disorders. *Trends Neurosci.* **2012**, *35* (3), 197−208.
(59) Potash, M. J.; Chao, W.; Bentsman, G.; Paris, N.; Saini, M.; Nitkiewicz, J.; Belem, P.; Sharer, L.; Brooks, A. I.; Volsky, D. J. A mouse model for study of systemic HIV-1 infection, antiviral immune responses, and neuroinvasiveness. *Proc. Natl. Acad. Sci. U. S. A.* **2005**, *102* (10), 3760−3765.
(60) Kim, B. H.; Kelschenbach, J.; Borjabad, A.; Hadas, E.; He, H.; Potash, M. J.; Nedelcovych, M. T.; Rais, R.; Haughey, N. J.; McArthur, J. C.; Slusher, B. S.; Volsky, D. J. Intranasal insulin therapy reverses hippocampal dendritic injury and cognitive impairment in a model of HIV-associated neurocognitive disorders in EcoHIV-infected mice. *Aids* **2019**, *33* (6), 973−984.
(61) Tarsa, L.; Goda, Y. Synaptophysin regulates activity-dependent synapse formation in cultured hippocampal neurons. *Proc. Natl. Acad. Sci. U. S. A.* **2002**, *99* (2), 1012−1016.
(62) Haga, H.; Yan, I. K.; Borrelli, D. A.; Matsuda, A.; Parasramka, M.; Shukla, N.; Lee, D. D.; Patel, T. Extracellular vesicles from bone marrow-derived mesenchymal stem cells protect against murine hepatic ischemia/reperfusion injury. *Liver Transpl.* **2017**, *23* (6), 791−803.
(63) Rodriguez, M.; Owens, F.; Perry, M.; Stone, N.; Soler, Y.; Almohtadi, R.; Zhao, Y.; Batrakova, E. V.; El-Hage, N. Implication of the Autophagy-Related Protein Beclin1 in the Regulation of EcoHIV Replication and Inflammatory Responses. *Viruses* **2023**, *15* (9), 1923.
(64) Murphy, A. J.; Kelschenbach, J.; He, H.; Chao, W.; Kim, B.-H.; Volsky, D. J.; Berman, J. W. Buprenorphine reverses neurocognitive impairment in EcoHIV infected mice: A potential therapy for HIV-NCI. *Front. Immunol.* **2022**, *13*, 1004985.
(65) Kaul, M.; Garden, G. A.; Lipton, S. A. Pathways to neuronal injury and apoptosis in HIV-associated dementia. *Nature* **2001**, *410* (6831), 988−994.
(66) Ogedengbe, O. O.; Saliu, H.; Fafure, A. A.; Akintayo, C. O.; Adekeye, A. O.; Ajiboye, B. O.; Azu, O. O. Hippocampus and Prefrontal Cortex Following the Use of Anti-Retroviral Therapy in Adult Wistar Rats: Therapeutic Role of Epigallocatechin Gallate. *Niger. J. Physiol. Sci.* **2023**, *37* (2), 207−214.
(67) Honeycutt, J. B.; Wahl, A.; Files, J. K.; League, A. F.; Yadav-Samudrala, B. J.; Garcia, J. V.; Fitting, S. In situ analysis of neuronal injury and neuroinflammation during HIV-1 infection. *Retrovirology* **2024**, *21* (1), 11.
(68) Schlachetzki, J. C. M.; Zhou, Y.; Glass, C. K. Human microglia phenotypes in the brain associated with HIV infection. *Curr. Opin. Neurobiol.* **2022**, *77*, 102637.
(69) Pokharkar, V.; Patil-Gadhe, A.; Palla, P. Efavirenz loaded nanostructured lipid carrier engineered for brain targeting through intranasal route: In-vivo pharmacokinetic and toxicity study. *Biomed. Pharmacother.* **2017**, *94*, 150−164.
(70) Pabst, R. Mucosal vaccination by the intranasal route. Nose-associated lymphoid tissue (NALT)—Structure, function and species differences. *Vaccine* **2015**, *33* (36), 4406−4413.

https://doi.org/10.1021/acsanm.4c04637
ACS Appl. Nano Mater. 2025, 8, 6857−6876